Journal Pre-proof

Independent and complementary bio-functional effects of CuO and Ga_2O_3 incorporated as therapeutic agents in silica- and phosphate-based bioactive glasses

T. Tite, A.C. Popa, B.W. Stuart, H.R. Fernandes, I.M. Chirica, G.A. Lungu, D. Macovei, C. Bartha, L. Albulescu, C. Tanase, S. Nita, N. Rusu, D.M. Grant, J.M.F. Ferreira, G.E. Stan

PII: S2352-8478(21)00181-7

DOI: https://doi.org/10.1016/j.jmat.2021.12.009

Reference: JMAT 531

To appear in: *Journal of Materiomics*

Received Date: 15 November 2021

Revised Date: 23 December 2021

Accepted Date: 28 December 2021

Please cite this article as: Tite T, Popa AC, Stuart BW, Fernandes HR, Chirica IM, Lungu GA, Macovei D, Bartha C, Albulescu L, Tanase C, Nita S, Rusu N, Grant DM, Ferreira JMF, Stan GE, Independent and complementary bio-functional effects of CuO and Ga_2O_3 incorporated as therapeutic agents in silica- and phosphate-based bioactive glasses, *Journal of Materiomics*, https://doi.org/10.1016/j.jmat.2021.12.009.

Independent and complementary bio-functional effects of CuO and Ga_2O_3 incorporated as therapeutic agents in silica- and phosphate-based bioactive glasses

T. Tite[a], A.C. Popa[a], B.W. Stuart[b], H.R. Fernandes[c], I.M. Chirica[a], G.A. Lungu[a], D. Macovei[a], C. Bartha[a], L. Albulescu[d], C. Tanase[d], S. Nita[e], N. Rusu[e], D.M. Grant[b], J.M.F. Ferreira[c], G.E. Stan[a,*]

[a] *National Institute of Materials Physics, Magurele, RO-077125, Romania*
[b] *Advanced Materials Research Group, Faculty of Engineering, University of Nottingham, NG7 2RD, UK*
[c] *CICECO—Aveiro Institute of Materials, Department of Materials and Ceramics Engineering, University of Aveiro, 3810-193 Aveiro, Portugal*
[d] *"Victor Babes" National Institute of Research and Development in Pathology and Biomedical Sciences, Bucharest, RO-050096, Romania*
[e] *National Institute for Chemical Pharmaceutical Research and Development, Bucharest, RO-031299, Romania*

*****Correspondence:
george_stan@infim.ro; Tel.: +40-21-241-8128; Fax: +40-21-369-0177.

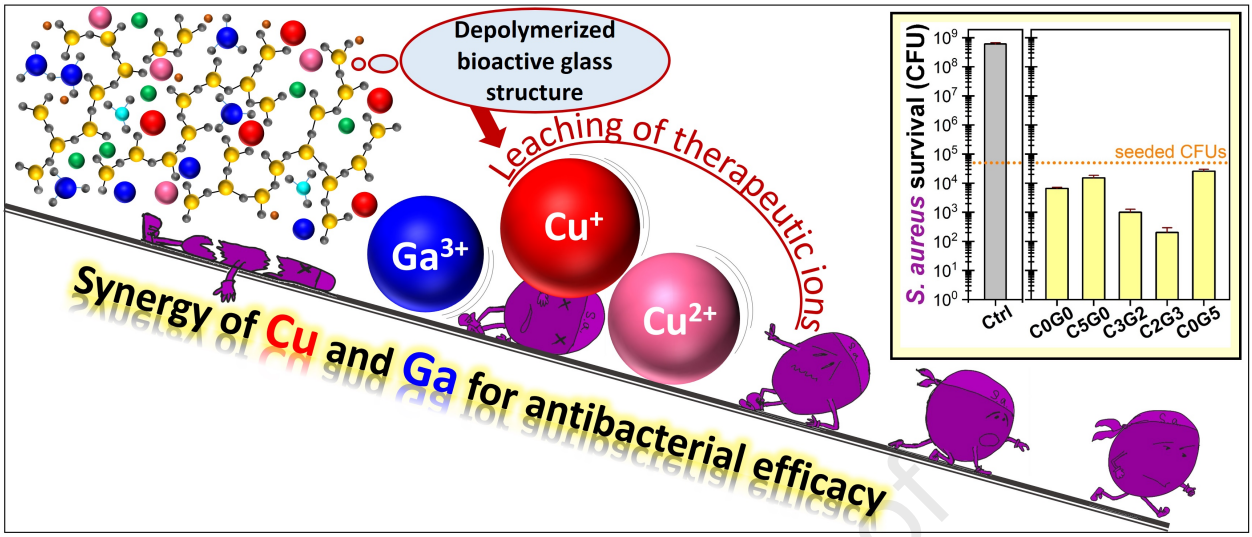

Independent and complementary bio-functional effects of CuO and Ga_2O_3 incorporated as therapeutic agents in silica- and phosphate-based bioactive glasses

T. Tite[a], A.C. Popa[a], B.W. Stuart[b], H.R. Fernandes[c], I.M. Chirica[a], G.A. Lungu[a], D. Macovei[a], C. Bartha[a], L. Albulescu[d], C. Tanase[d], S. Nita[e], N. Rusu[e], D.M. Grant[b], J.M.F. Ferreira[c], G.E. Stan[a,*]

[a] *National Institute of Materials Physics, Magurele, RO-077125, Romania*
[b] *Advanced Materials Research Group, Faculty of Engineering, University of Nottingham, NG7 2RD, UK*
[c] *CICECO—Aveiro Institute of Materials, Department of Materials and Ceramics Engineering, University of Aveiro, 3810-193 Aveiro, Portugal*
[d] *"Victor Babes" National Institute of Research and Development in Pathology and Biomedical Sciences, Bucharest, RO-050096, Romania*
[e] *National Institute for Chemical Pharmaceutical Research and Development, Bucharest, RO-031299, Romania*

Abstract: The incorporation of therapeutic-capable ions into bioactive glasses (BGs), either based on silica (SBGs) or phosphate (PBGs), is currently envisaged as a proficient path for facilitating bone regeneration. In conjunction with this view, the single and complementary structural and bio-functional roles of CuO and Ga_2O_3 (in the 2–5 mol% range) were assessed, by deriving a series of SBG and PBG formulations starting from the parent glass systems, FastOs®BG – $38.5SiO_2$—$36.1CaO$—$5.6P_2O_5$—$19.2MgO$—$0.6CaF_2$, and $50.0P_2O_5$—$35.0CaO$—$10.0Na_2O$—$5.0\ Fe_2O_3$ (mol%), respectively, using the process of melt-quenching. The inter-linked physico-chemistry – biological response of BGs was assessed in search of bio-functional triggers. Further light was shed on the structural role – as network former or modifier – of Cu and Ga, immersed in SBG and PBG matrices. The preliminary biological performance was surveyed *in vitro* by quantification of Cu and Ga ion release under homeostatic conditions, cytocompatibility assays (in fibroblast cell cultures) and antibacterial tests (against *Staphylococcus aureus*). The similar (Cu) and dissimilar (Ga) structural roles in the SBG and PBG vitreous networks governed their release. Namely, Cu ions were leached in similar concentrations (ranging from 10–35 ppm and 50–110 ppm at BG doses of 5 and 50 mg/mL, respectively) for both type of BGs, while the release of Ga ions was 1–2 orders of magnitude lower in the case of SBGs (*i.e.*, 0.2–6 ppm) compared to PBGs (*i.e.*, 9–135 ppm). This was attributed to the network modifier role of Cu in both types of BGs, and conversely, to the network former (SBGs) and network modifier (PBGs) roles of Ga. All glasses were cytocompatible at a dose of 5 mg/mL, while at the same concentration the antimicrobial efficiency was found to be accentuated by the coupled release of Cu and Ga ions from SBG. By collective assessment, the most prominent candidate material for the further development of implant coatings and bone graft substitutes was delineated as the $38.5SiO_2$—$34.1CaO$—$5.6P_2O_5$—$16.2MgO$—$0.6CaF_2$—$2.0CuO$—$3.0Ga_2O_3$ (mol%) SBG system, which yielded moderate Cu and Ga ion release, excellent cytocompatibility and marked antibacterial efficacy.

Keywords: *bioactive glass; copper; gallium; structure; ion release; antibacterial.*

*****Correspondence:
george_stan@infim.ro; Tel.: +40-21-241-8128; Fax: +40-21-369-0177.

1. Introduction

In recent years, the orthopaedic and dentistry fields experienced an unprecedented demand for innovative and highly efficacious biomaterials, capable not only of overcoming the deficient bone bonding ability of metallic (*e.g.*, titanium and titanium super-alloys) implants, but also of tackling the continually increasing incidence of post-surgery infections attributed to the rise of resistant bacterial stains [1–4].

In this context, bioactive glasses (BGs), classified according their dominant network former oxide into silica- (SBGs), phosphate- (PBGs), and borate-based (BBGs) glasses, could unlock new avenues for tissue engineering, due to their unique physical-chemical properties, promising biological responses (*e.g.*, excellent biocompatibility, osseointegration) [5–7], and fascinating ability to accommodate various metallic ions with antimicrobial/antifungal properties within their structure [5–8].

The story of BGs, started with Prof. Hench and his collaborators [9] which remoulded the perception of glasses in bone tissue engineering, transforming a rather mundane material into one of the most fashionable and alluring in healthcare. The original BG formulation (mol%: 46.1SiO_2–24.4Na_2O–26.9CaO–2.6P_2O_5), commonly denominated as 45S5, was shown to facilitate fast bone bonding [5,6,10], and currently it is commercialized under various trademarks (*e.g.*, Bioglass®, Biogran®, NovaBone®, NovaMin®, Perioglas®, TeraSphere®) [6,11]. Over the course of years, 45S5 has been used as a benchmark for the fabrication of new SBG formulations with added bio-functional traits (*e.g.*, angiogenesis, antimicrobial effect) [6,7,11]. Noteworthy are also the studies moving towards the decrease or even elimination of alkalis from SBGs [12–14], as their presence is known to be in many cases detrimental (*e.g.*, burst release, unpredictable degradation, high reactivity, steep pH increase, which occasionally could impose preconditioning stages [6,7,15]). Nowadays, the delineation of biologically effective BGs constitutes a hot research topic in full swing, with the focus expanding towards both PBGs (more markedly) [4,16,17] and BBGs (more recently) [18–20] compositions.

Regardless, of their glass network matrix, BGs are expected to become noteworthy candidates for translation into biomedical applications, either as bone graft substitutes (scaffolds) or as (long-lasting or sacrificial temporary) coatings for the bio-functionalization of metallic implants [6,16,21,22]. In this context, effective strategies for modifying the chemistry and structure of BGs are sought to increase their biological performance, with all glass constituents (*i.e.*, *network*

formers, *modifiers and intermediates*) being scrutinized [6,23]. Whether we consider the (*i*) SBGs, as the materials with the most potent biomineralization capacity (*e.g.*, generation of carbonated HA layers in contact with body fluids) fit for bone graft substitutes and adherent coatings for endo-osseous cementless implants [6], or the (*ii*) PBGs, in the P_2O_5–CaO–Na_2O system, as fast biodegradable materials [24–26] suitable as a therapeutic ion reservoir for drug delivery systems and sacrificial thin films capable of boosted short-lived biological effects [24,27], the leaching kinetics of the beneficial ions depends on the glass network structure and ions' role as *network former*, *modifier* or *intermediate*. This is why, a better understanding of the interlinks between structural role and performance under near-real biological condition, in the case of SBGs and PBGs, could open a myriad of possibilities for using such materials, standalone or combined, for advanced healthcare applications.

Recently, the individual incorporation of antimicrobial agents (*e.g.*, silver, zinc, copper, or gallium) in BGs has been recognised as a new attractive strategy for boosting their bio-functionality, aiming to reduce the increasing number of post-surgery infections [6,28,29]. The combined action of such antimicrobial agents (if possessing different underlying mechanisms), incorporated into BGs, is expected to expand their therapeutic range. In exploring and developing this vision, two promising antimicrobial elements – copper (Cu) and gallium (Ga) – were selected herein, and were separately and concurrently incorporated into SBG and PBG formulations, and comparatively studied.

Copper has long been used as antibacterial agent in biomedical research [30,31] and, has riveted in recent years since Cu surfaces exclusively passed the new US EPA test protocol in 2008 [32,33]. Different studies showed that Cu incorporated BGs can reduce both Gram-positive and Gram-negative bacterial strains. For instance, Gross *et al.* doped melt-quenched SBGs with Cu ions by an ion-exchange process, and obtained excellent antimicrobial efficiency (99.9% reduction) against *Pseudomonas aeruginosa*, *Escherichia coli*, *Klebsiella aerogenes* and *Staphylococcus aureus* [32]. Furthermore, Liu *et al.* have employed biodegradable Cu-doped phosphate-based glass (Cu-PBG) nanozymes for the controlled release of Cu ions to eradicate *S. aureus* and *E. coli* bacteria [30]. *E. coli* and *S. aureus* strains were reduced at Cu-PBG concentration of 0.3 mg/mL down to 54.9% and 51.2%, respectively, while for a dose of 0.5 mg/mL the extermination values reached 95.1 and 94.0 %, respectively. The antibacterial mechanism of Cu is believed to be related to its ability to (*i*) generate reactive oxygen species

(ROS) and reactive hydroxyl radicals to directly damage the cell membrane through Fenton-type reaction or enzyme activity (*e.g.*, peroxidase (POD)-like activity), and to (*ii*) denature DNA/RNA by ion chelating after entering the cells. Other prominent biological features of Cu-doped BGs include an improvement in cell proliferation and promotion of angiogenesis [6,11].

Gallium, FDA approved to treat hypercalcemia of malignancy [34], has emerged as a potent antimicrobial element to defeat drug-resistant bacteria thanks to a "Trojan horse" effect against the iron-seeking bacteria [35–37]. Because of its similarity to Fe^{3+} ion (*e.g.*, almost identical ionic radius, coordination number, and ionization potential) [35,36], Ga^{3+} ions enter bacteria through Fe^{3+} uptake systems, disrupting the Fe metabolism and the function of some Fe-containing proteins, leading to the inhibition of bacteria growth/biofilm formation. Ga-substituted SBGs proved to be effective against both Gram-positive (*S. aureus* [4,38]) and Gram-negative bacteria (*E. coli* [4,38], *P. aeruginosa* [36]). Similar promising antimicrobial effects were also found for Ga-substituted PBGs [34,39]. Antibacterial efficacy was reported for melt-quenched PBG with Ga_2O_3 concentration as low as 1 mol% [34]. Recently, the antibacterial activity of Ga-PBG films deposited by magnetron sputtering has been reported (*i.e.*, a 5-log and 6-log reduction of *E. coli* and *S. aureus*, after 24 h), with the strength of the effect being controlled by the layer thickness [4]. This suggested the possibility to respond with more specificity to patient needs (along with a diminution of side effects) by tuning the amounts of therapeutic ions to be released and thereby, the duration and intensity of the antimicrobial activity.

To the best of our knowledge, only few attempts to endow bioactive glasses with superior therapeutic effects (*e.g.*, osseointegration, angiogenic, wound healing, and antimicrobial effects), by dual- or multi-oxide substitutions have been reported so far, amongst them: Ce-Ga in both PBGs and SBGs [35,40], and Zn-Sr [14,41], Ag-Mn [42], and Ag-Co-Ti [43] in SBGs. In the study herein, the incorporation of both Cu and Ga in well-established SBG and PBG systems was explored from physico-chemical and preliminary biological standpoints, as a facile and safe solution to boost the antimicrobial efficacy of these biomaterials. Particular attention was devoted to understanding the structural role of gallium in SBGs and PBGs, as it could prove to be of high importance for the predictability of their biological performance.

2. Materials and Methods

2.1 Preparation of bioactive glass powders with/without antibacterial agents

Ten formulations of SBGs (based on the FastOsBG® system [44]) and PBGs (derived from the P_2O_5–CaO–Na_2O–Fe_2O_3 compositional system, proposed in Ref. [16]) were prepared by melt-quenching. Their expected/theoretical oxide concentrations (in mol%) and corresponding sample codes are presented in Table 1. CuO partially substituted CaO (for both SBG and PBG systems), whilst Ga_2O_3 partially replaced MgO (for SBGs) or Fe_2O_3 (for PBGs). The substitutions were performed considering not the valence of the respective ion, but its consecrated structural role as network modifier (Ca in both SBGs and PBGs) [45,46] or intermediate (Mg in SBGs [47] and Fe in PBGs [48]). This could allow to infer the single and coupled structural and biofunctional roles of Cu and Ga in these two types of glass matrices. Furthermore, this way, the excessive depletion of network modifier Ca (for both SBGs and PBGs) and the diminution (in the case of PBGs) or close to total reduction of the network former P (in the case of SBGs), two elements that play a decisive role in the biological response of BGs, have also been avoided.

The SBGs were synthesized using the SiO_2, $CaCO_3$, CaF_2, NH_6PO_4, MgO, CuO (BDH Chemicals Ltd., purity > 99%) and/or Ga_2O_3 (ThermoFisher Scientific, purity 99.99%) precursors, by applying the preparation protocol reported in Ref. [14]. In the case of PBGs, the procedure described in Ref. [16] was used, employing the following precursors: P_2O_5 (ThermoFisher Scientific, purity >99%), $CaHPO_4$, NaH_2PO_4, $FePO_4{\cdot}2H_2O$, CuO (purity >99%) and/or Ga_2O_3 (Sigma Aldrich, purity >99.99%). The as-prepared bulk glasses were ground using an agate ball mill and sieved through a 63 μm mesh size to obtain fine powders.

Table 1: *The oxide concentration (in mol%) – theoretical (the.) and experimentally (exp.) determined by EDXS as arithmetic means ± standard deviation (n=3) – and thermal parameters (extracted on the basis of the TG–DSC measurements) of the as-synthesized SBG and PBG materials. *Note: The fluorine content could not be accurately quantified, being too close to its EDXS detection limit.*

Sample code		Oxide concentration (mol %)							Thermal properties		
SBG series		SiO_2	CaO	P_2O_5	MgO	CaF_2*	CuO	Ga_2O_3	T_g (°C)	T_c (°C)	T_m (°C)
C0G0	the.	38.5	36.1	5.6	19.2	0.6	–	–	715	912	>1200
	exp.	39.3±0.2	36.7±0.6	5.0±0.1	19.0±0.3	–	–	–			
C5G0	the.	38.5	31.1	5.6	19.2	0.6	5.0	–	694	881	1161
	exp.	38.7±0.5	32.2±0.4	5.1±0.1	18.4±0.2	–	5.6±0.9	–			

C3G2	the.	38.5	33.1	5.6	17.2	0.6	3.0	2.0	657	897	>1200
	exp.	38.6±0.3	33.9±1.0	5.2±0.1	16.8±05	–	3.6±0.5	1.9±0.1			
C2G3	the.	38.5	34.1	5.6	16.2	0.6	2.0	3.0	721	895	>1200
	exp.	38.7±0.3	34.7±0.7	5.1±0.1	16.1±0.4	–	2.6±0.4	2.8±0.1			
C0G5	the.	38.5	36.1	5.6	14.2	0.6	–	5.0	800	938	>1200
	exp.	39.6±0.4	36.6±0.8	5.0±0.2	14.0±0.2	–	–	4.8±0.1			
PBG series		**P_2O_5**	**CaO**	**MgO**	**Na_2O**	**Fe_2O_3**	**CuO**	**Ga_2O_3**	***T_g (°C)***	***T_c (°C)***	***T_m (°C)***
C0G0	the.	50.0	35.0	–	10.0	5.0	–	–	561	686	811
	exp.	49.8±0.4	33.7±0.2	–	12.3±0.3	4.2±0.1	–	–			
C5G0	the.	50.0	30.0	–	10.0	5.0	5.0	–	530	680	804
	exp.	48.9±0.1	29.3±0.2	–	11.4±0.1	4.8±0.1	5.6±0.1	–			
C3G2	the.	50.0	32.0	–	10.0	3.0	3.0	2.0	440	688	790
	exp.	48.4±0.1	31.7±0.2	–	11.6±0.4	3.0±0.1	3.2±0.2	2.1±0.1			
C2G3	the.	50.0	33.0	–	10.0	2.0	2.0	3.0	518	684	785
	exp.	50.0±0.2	32.2±0.4	–	10.0±0.4	2.0±0.1	2.2±0.1	3.6±0.3			
C0G5	the.	50.0	35.0	–	10.0	–	–	5.0	457	609	1185
	exp.	50.5±0.1	34.4±0.2	–	9.9±0.2	–	–	5.2±0.1			

2.2 Physico-chemical characterisation techniques

(*a*) The compositions of the as-prepared BGs were verified by energy dispersive X-ray spectroscopy (EDXS) using an Oxford Instruments apparatus attached to a Phillips XL30 scanning electron microscope (SEM), at an acceleration voltage of 15 kV. The measurements were performed over (at least three randomly chosen) specimen regions with areas of 250 × 250 μm^2. Since the quantification of lighter elements (*i.e.*, oxygen and fluorine) by EDXS is prone to large errors, it was disregarded. The as-determined elemental concentrations of Si, Ca, P, Mg, Na, Fe, Cu and Ga (at.%) were converted to mol% oxide compositions, considering the stoichiometric molecular formulas, with oxygen as minuend. The BGs oxide concentrations have been presented as arithmetic means ± standard deviations.

(*b*) The thermal analyses were performed with a Setaram Setsys Evolution 18 instrument in a Thermogravimetry – Differential Scanning Calorimetry (TG–DSC) mode, from room temperature up to 1200 °C. The powder samples (~25 mg) were measured in synthetic air (80%

N_2/20% O_2; gas flow rate of 16 mL/min) at a heating rate of 10 °C/min. The accuracy of the heat flow measurements and temperature precision were of ± 0.001 mW and ± 0.1 °C, respectively.

(*c*) The amorphous state of the SBG and PBG powders was verified by X-ray diffraction (XRD), in the angular range 2θ from 15 to 60°, with a step size of 0.04°, and a dwell time of 3 s, using a Bruker D8 Advance diffractometer ($CuK_{\alpha,}$ λ=1.5418 Å) set in Bragg-Brentano geometry.

(*d*) The chemical structure and the bonding arrangement of the SBG and PBG materials was investigated by Fourier transform infrared spectroscopy (FTIR) spectroscopy in transmission mode (on pressed pellets with a BG:KBr mass ratio of 1:150), using a Perkin Elmer Spectrum BX II spectrophotometer. The spectra were acquired in the wave numbers range of 4000–400 cm^{-1}, at a resolution of 4 cm^{-1}.

(*e*) The chemical state of Cu and Ga in selected SBG and PBG materials was examined by X-ray photoelectron spectroscopy (XPS) using a Specs GmbH Multimethod System, equipped with a Phoibos 150 hemispherical energy analyser with a multi-element two-stage transfer lens and a nine channeltrons detector array. The photo-emission studies have been carried out at a pressure of ~10^{-7} Pa, using a XR-50M Mg K_α (1253.6 eV) source, set at 300 W. A pass energy of 20 eV was used for the high-resolution core level spectral recordings. The sample neutralization during the measurements was achieved by using a flood gun, working at acceleration energy of 1 eV and an emission current of 0.1 mA. The spectra were charge corrected with respect to adventitious carbon (284.8 eV). The fitting of spectra was performed with a dedicated software Spectral Data Processor using Voigt functions, and a Shirley background.

(*f*) The Ga local environment of selected SBG and PBG materials was investigated by extended X-ray absorption fine structure (EXAFS) spectroscopy. The primary absorption spectra were acquired in fluorescence mode at the Ga K edge (10367 eV) with a laboratory-grade Rigaku EXAFS spectrometer [49,50], between ~300 eV before the edge and 650 eV above it, with a 2 eV step in the EXAFS range. The continuous radiation of an X-ray tube with molybdenum target was analysed on a curved Ge(220) single-crystal monochromator. The absorbing samples, finely powdered and pressed as pellets, were placed between a proportional Ar-filled counter and a solid-state detector, which measured the intensities of the incident and fluorescence X-ray beams, respectively. After subtraction of pre-edge and post-edge backgrounds from the spectra, the EXAFS function $\chi(k)$ (k = photoelectron wave number) was calculated from the post-edge oscillations of the spectra, normalized through the smooth atomic absorption (post-edge

background). The $k^3\chi(k)$ spectra were then Fourier transformed over the k range ~2–13 Å^{-1}. The Fourier transforms (FT) of EXAFS approximate radial distribution functions around the absorbing Ga atoms, with maxima corresponding, up to systematic shifts, to the neighbouring shells of Ga. The first main maximum of FT, corresponding to the nearest oxygen neighbours of Ga was further isolated by a Hanning-function window, backtransformed into *k*-space (Fourier filtering) and non-linearly fitted by a least-square method. The fit of the filtered EXAFS provided the number of the nearest oxygen neighbours of Ga, the interatomic Ga–O distance, and the degree of structural disorder of the neighbouring oxygen shell. The processing of the primary data for calculation of the EXAFS function $\chi(k)$ was carried out by using the Athena program [51], whereas the fit of EXAFS was done with the Artemis package, including the ATOMS, FEFF and IFEFFIT routines [51–55].

2.3 In vitro biological assays

Three independent quantities of 0.1, 0.02 and 0.01 g of each composition of powder, were weighed with a micro-balance with an accuracy of 10^{-4} g. Prior to the *in vitro* assays, all SBGs and PBGs, precisely weighted and placed in the relevant biological sealed testing vials, were sterilized by gamma irradiation at the Multipurpose Irradiation Facility Centre, within the "Horia Hulubei" National Institute for R&D in Physics and Nuclear Engineering, Romania. The minimum absorbed dose was 25 kGy.

To allow for a homogeneous, straightforward cross-interpretation of biological testing results, the (*a*) pH measurements, (*b*) therapeutic ion release, and (*c*) cytocompatibility assays, were performed in the same medium used for the cell culture tests, namely the Dulbecco′s Modified Eagle′s Medium/Nutrient Mixture F-12 Ham (code D6421, Sigma Aldrich) with 15 mM of HEPES (4-(2-hydroxyethyl)-1-piperazineethanesulfonic acid) buffer agent and sodium bicarbonate, supplemented with L-glutamine and 10% foetal bovine serum (FBS), further denoted DMEM/F12-FBS, and not in conventional inorganic solutions such as Kokubo's simulated body fluid (SBF) or Tris-HCl (as suggested in ISO 10993–14). It is to note, that currently, an active, and rather constructive, debate is taking place worldwide on the most suitable testing environments for acellular *in vitro* tests [56–59], whether we're talking about degradation/ion release (topical in the context of this study), bioactivity/mineralization or corrosion testing. Several critical aspects need to be considered for reliable testing, amongst which, of great most important are: (*i*) ensuring

faithful/realistic biomimetic conditions (although it seems straightforward, not many today's studies adopt the correct biomimetic conditions – 5% CO_2, 37 °C, humidified ambient, preferring a normal dry ambient), and (*ii*) suitable choice of acid-base buffering systems. Without such prerequisites, abnormal/drastic pH modifications of media occur, having as consequences the pronounced glass degradation, burst release of ions, and even the undesirable formation of $CaCO_3 \cdot H_2O$, $CaCO_3$ and NaCl crystalline phases (kinetically favoured at high pH values), irrespective of testing medium (*e.g.*, SBF, DMEM) [56,57,59].

Two mL of DMEM/F12-FBS medium were added to the sterilized vials containing 0.1 and 0.01 g of each type of SBG or PBG, leading to two *"BG mass/testing medium volume"* ratios of 50 and 5 mg/mL, respectively. The samples were kept for 24 h under agitation in an incubator under homeostatic conditions (5% CO_2, 37 °C, humidified ambient). Subsequently, the tubes were centrifuged (at 700 × *g*), and the liquid was separated from the remaining powder. The extracted medium was filtered through a 0.22 μm Millipore™ membrane filter, and then stored in sealed containers in the refrigerator (at 4 °C), up to maximum 24 h, to prevent evaporation and contamination, until the debut of experiments.

(*a*) *pH measurements*

A part of the extracted medium was used for pH measurements using a LAQUAtwin pH-33 apparatus. Before each set of measurements, the pH meter was calibrated in USA buffers (model no. 502-S) with pH values of 7.00 and 4.01, followed by the rinse of the pH-meter electrode in deionised water and drying.

(*b*) *Therapeutic ion release determinations*

Another part of the medium was diluted by a factor of 100 with ultra-pore Milli-Q™ water to curtail the plasma instability and non-spectral interferences which could be induced by the abundant organic moieties present in DMEM/F12-FBS. Then, the ionic concentrations (in mg/L, multiplied by the dilution factor) of the therapeutic ions of interest (*i.e.*, Cu and Ga) were determined by inductively coupled plasma mass spectroscopy (ICP-MS), employing a PerkinElmer ELAN DRC-e quadrupole-based system.

(c) Cytocompatibility assessments

In vitro cytocompatibility experiments of SBG and PBG were performed in accordance with the specifications of the ISO 10993-5:2009 standard: "*Biological evaluation of medical devices* –

Part 5: Tests for in vitro cytotoxicity". The *in vitro* cell culture protocol is succinctly described hereunder:

Cell culture

NIH/3T3 mouse fibroblasts were grown in the DMEM/F12-FBS at 37 °C and 5% CO_2 and passaged every 2–3 days.

Cell viability/proliferation and cell death assays

The cytocompatibility of the SBG and PBG powders was evaluated by cell viability (by *3-(4,5-dimethylthiazol-2-yl)-5-(3-carboxymethoxyphenyl)-2-(4-sulfophenyl)-2H-tetrazolium* (MTS) *assay*) and cell death (by the *lactate dehydrogenase* (LDH) *assay*) testing, using a NIH/3T3 mouse fibroblast cell line (ATCC® CRL-1658™).

The NIH/3T3 cells were seeded in 96-well at 5000 cells/well and allowed to attach and proliferate for 24 h, after which the medium was replaced with SBG or PBG conditioned media and incubated for another 24 h. The proliferation was assessed using MTS according to the manufacturer's (Promega Corporation) protocol. Supernatants from these cells were used to assess cell death by the LDH test (CytoTox 96® non-radioactive cytotoxicity assay kit) according to the manufacturer's (Promega Corporation) protocol.

(d) Antibacterial tests

The antibacterial tests were performed in suspension in a nutrient broth medium (meat peptone, meat extract, NaCl – 5 g/L each, produced by Sanimed International Impex, certified supplier for medical bacteriology laboratories). The Gram-positive bacterial strain *S. aureus* (ATCC® 6538) was used. An inoculum of bacterial cells was prepared and the number of colony forming units (CFU) in the inoculum were determined (colonies were quantified 24 h after serial dilutions and then mounted on soft agar). To each round bottom flask containing 0.02 g of the sterile SBG and PBG powders were added 4 mL of nutrient broth containing 10^5 CFU/mL, resulting in *"BG mass/testing medium volume"* ratio of 5 mg/mL. The flasks were then stored in an incubator at 37 °C on an orbital shaker at 250 rpm. After 24 h the specimens were subjected to the procedure for determining the viable CFUs. For this purpose, the samples were vortexed (1 min at 1200 rpm) and then serial dilutions were prepared. From each dilution, two aliquots of 1 mL were evenly distributed on the agar plates. The plates were placed in the incubator, and after 24 h, the colonies were counted. The CFU value was calculated using the equation: CFU = (mean number of colonies) × (dilution factor).

(d) Statistical analysis

All *in vitro* biological measurements/assays were performed in triplicate and the data will be presented as arithmetic means ± standard deviations. A statistical analysis was performed using a one-way ANOVA multiple analysis comparison followed by a Dunnett's post hoc test, with the differences being considered significant when $p < 0.05$.

3. Results

3.1 Physico-chemical determinations

3.1.1 EDXS

The composition of the melt-quenched BGs was inferred by EDXS, and the planned and experimental oxide compositions are given in Table 1. It can be concluded that the anticipated SBG and PBG formulations have been obtained (including the concentrations of therapeutic agents) within the experimental errors [60].

3.1.2 Thermal analysis

The glass transition (T_g), crystallization (T_c) and melting (T_m) temperatures of the studied glasses are presented in Table 1. Higher T_c and T_m values have been consistently obtained for SBGs with respected to PBGs, denoting the better structural thermal stability of the former, and providing a series of indications regarding their possible processing window in the form of glass-ceramic implant coatings and scaffolds. The expansion and weakening of the glass network are characteristically accompanied by a decrease in T_g [61]. On the overall, in the case of SBGs, the incorporation of Cu produced a decline of the T_g (suggesting its prominent network modifier role), whilst Ga incrementally increased the T_g (implying its foremost network former role). However, for PBGs, both Cu and (more markedly) Ga induced a decrease of the T_g. This provided a first clue that Ga plays dissimilar structural roles in the SBG and PBG networks.

3.1.3 XRD

The XRD patterns of the glasses in the SBG and PBG series are comparatively shown in Fig. 1. These analyses confirmed the amorphous character of all SBG and PBG materials, regardless of their composition. The XRD diagrams of SBG powders are characterized by a halo centred at $2\theta \approx 29°$ (Fig. 1a), typical for moderately depolymerized glasses [14]. The amorphous halo of the PBG materials was found to be located at $2\theta \approx 25°$ (Fig. 1b), being thus displaced to lower angles. The diffraction halo is related to radii of the first coordination spheres (determined

by the bond lengths and angles) and thereby, the average distances between atoms in the amorphous compound. The lower intensity and broader aspect of the PBGs halos suggested their increased structural disorder with respect to SBGs. The down-shift of the halo position in the case of PBGs indicated a more rarefied glass network with lower packing density. Consequently, it is expected for the PBG materials to be more readily solubilized than SBGs, and able to release therapeutic ions within at higher rates.

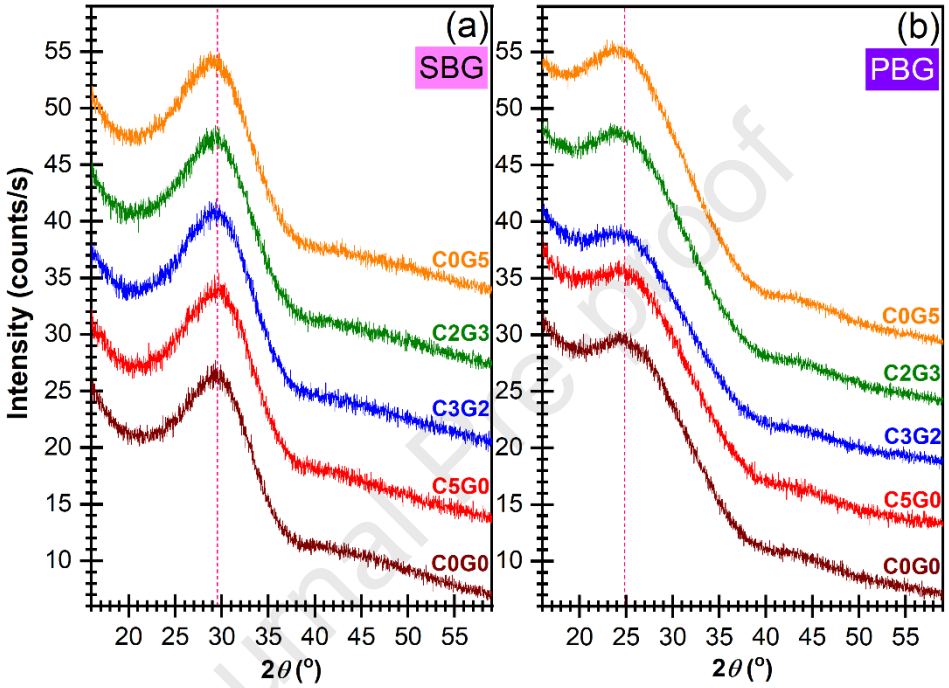

Figure 1: *The characteristic XRD diagrams, collected in Bragg-Brentano geometry, of the (**c**) SBG and (**d**) PBG powders, with and without CuO and/or Ga_2O_3 therapeutic agents.*

3.1.4 FTIR spectroscopy

The FTIR spectra of the SBG and PBG compositional systems are comparatively presented in Fig. 2. The progressive incorporation of network modifiers will decrease the connectivity of the silicate or phosphate network since the cation electric charge can only be compensated by the fracture of the oxygen bridges (BO) corner-shared by the silicate (Q_{Si}^4) and ultraphosphate (Q_P^3) structural units. Consequently, the number of non-bridging oxygen (NBO) of the glass will be increased, generating in an incremental manner Si–1NBO (Q_{Si}^3), Si–2NBO (Q_{Si}^2), Si–3NBO (Q_{Si}^1) and Si–4NBO (Q_{Si}^0) tetrahedra for SBGs, and P–2NBO (Q_P^2), P–3NBO (Q_P^1) and P–4NBO (Q_P^0) units for PBGs. A lower degree of network connectivity is known to favour the glass solubility in

physiological environments, and to accommodate an efficient release of therapeutic ions within their structure [62,63].

The FTIR spectra of SBGs (Fig. 2a) elicited a high degree of similarity and were characterized by the presence of two prominent and broad IR absorption bands, positioned in the wave number regions of 1400–800 cm^{-1} and 650–400 cm^{-1}. The first IR band is marked by four defined shoulders, peaking at *ca.* (*i*) 1181, (*ii*) 1032, (*iii*) 950, and (*iv*) 855 cm^{-1}, and appertaining to the asymmetric stretching (ν_{as}) vibrations of the Si–O–Si bonds in all silicate tetrahedral units (the (*i*) longitudinal LO_3 and (*ii*) transverse TO_3 optical modes), and to ν_{as} of Si–NBO bonds in (*iii*) Q_{Si}^3 and Q_{Si}^2 and (*iv*) Q_{Si}^1 and Q_{Si}^0 units, respectively [14,58,64–66]. The maxima positioned at ~562 and 506 cm^{-1} belong to the bending (δ) and rocking (ρ) vibration modes of Si–O bonds in all silicate groups [58,64,65]. The IR bands of phosphate groups are difficult to pinpoint for SBGs, due to the overlap in the same spectral range of the intense vibration modes generated by the prominent silicate groups [65]. The similar intensity ratio of the Si–O–Si and Si–NBO absorption bands indicated analogous moderate degrees of connectivity for the SBGs with different compositions.

In the case of PBGs (Fig. 2b), the FTIR spectra featured a series of well-defined IR maxima, similar in position and amplitude, and highly specific to phosphate glasses with a low degree of connectivity [67–69]. They were centred at *ca.* (*i*) 1274, (*ii*) 1094, (*iii*) 1003, (*iv*) 907, (*v*) 748, (*vi*) 530, and (*vii*) 492 cm^{-1}, and are ascribed to the: ν_{as} of P–NBO bonds in the (*i*) middle-of-chain $(PO_2)^-$ (Q_P^2) and (*ii*) end-of-chain $(PO_3)^{2-}$ (Q_P^1) units; (*iii*) vibrations in isolated Q_P^0 structural units; (*iv*) ν_{as} of P–O–P bonds in Q_P^2 structural units; (*v*) symmetric stretching (ν_s) vibrations of P–O–P bonds in all Q_P^n structural units; bending (δ) of the (*vi*) P=O–P bonds, and (*vii*) linkages in the intermediate Q_P^2 groups [16,67,70]. Thus, it can be concluded that the PBGs structure consisted of a balanced mixture of phosphate structural units with two (Q_P^2) and three (Q_P^1) NBOs, which will render them rapidly biodegradable, allowing for an efficient release of the constituting therapeutic ions. A notable difference was ascertained: the incorporation of Ga_2O_3 in PBGs was accompanied by the emergence of the ν_{as} Q_P^0 band (~1003 cm^{-1}), testimony of a slight local depolymerisation of these glasses.

3.1.5 XPS

The X-ray photoelectron spectra of the Cu $2p_{3/2}$ and Ga $2p_{3/2}$ core electron levels collected for the SBG and PBG C2G3-type samples are shown in Figs. 2c and 2d, respectively. The Cu $2p_{3/2}$ spectra of both SBG and PBG glasses were analogous in both binding energy position and shape, denoting similar chemical states. Namely, the Cu $2p_{3/2}$ core electron levels featured a larger (~70%) component at ~932.7 eV ascribed to Cu^{1+} and a smaller (~30%) one at ~933.9 eV, attributed to Cu^{2+} [71,72]. The Cu^{2+} occurrence was supported also by the emergence of its characteristic shake-up satellites in form of a low intensity broad spectral peak situated in the binding energy region of ~938–946 eV [71,72]. The Ga $2p^{3/2}$ spectra of both SBG and PBG glasses were fitted with two components (A and B), corresponding to a lower (A) and a higher (B) oxidation state. Peaks A are located at similar binding energies for SBG-C2G3 (~1117.8 eV) and PBG-C2G3 (~1117.9 eV), whilst peak B is shifted to higher energy in the case of PBG-C2G3 (~1119.7 eV) with respect to SBG-C2G3 (~1119.0 eV), which is indicative of a higher oxidation state of the former (and denoting a richer oxygen chemical environment of Ga atoms) [72,73].

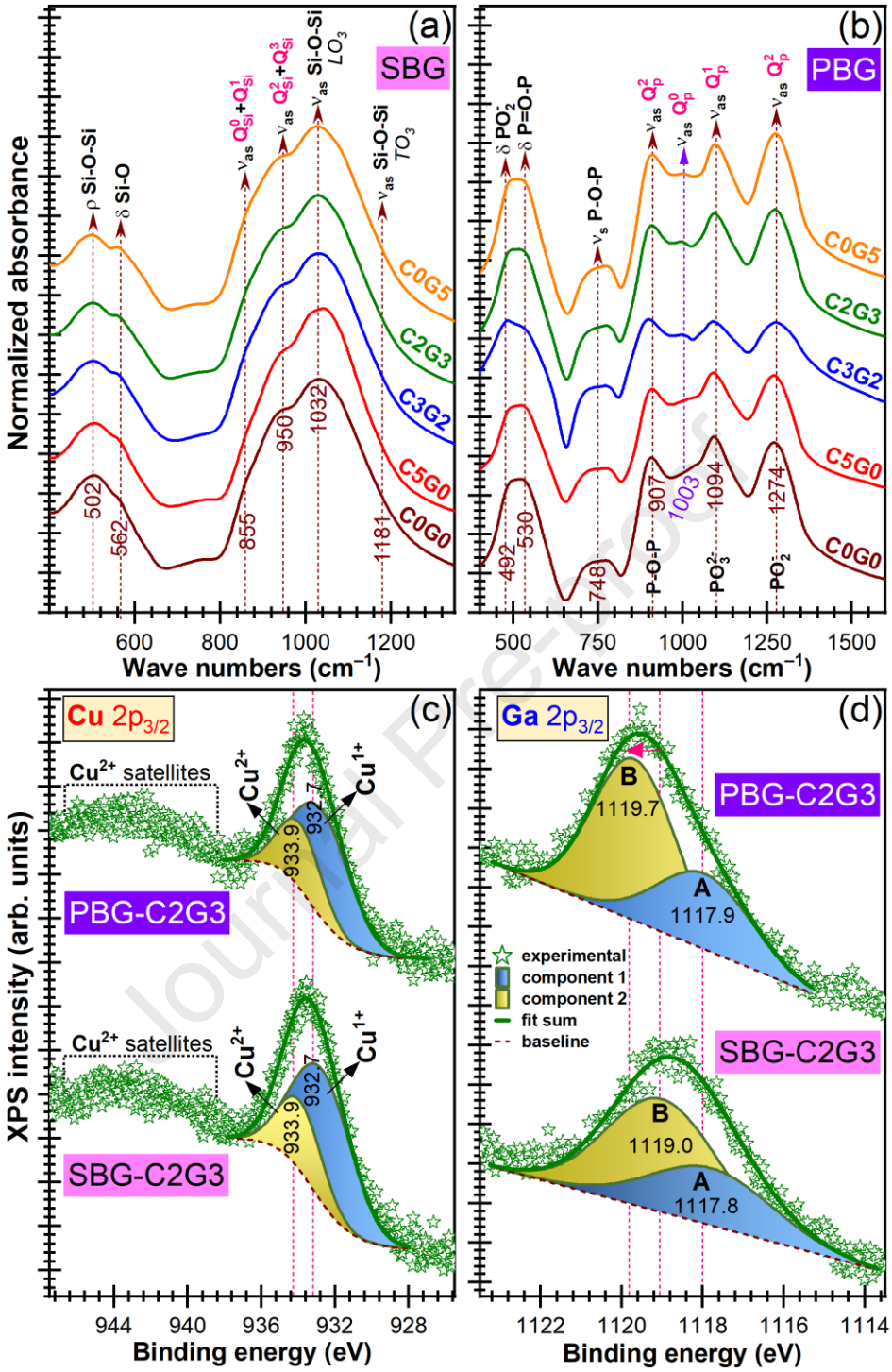

Figure 2: *Comparative FTIR spectra of the (**a**) SBG and (**b**) PBG materials, with and without CuO and/or Ga_2O_3 therapeutic agents. High resolution XPS spectra of the (**c**) Cu $2p_{3/2}$ and (**d**) Ga $3p_{3/2}$ core photoelectron levels recorded in the case of the Cu and Ga substituted SBG and PBG C2G3-type materials.*

3.2 In vitro bio-functional evaluation

3.2.1 pH and therapeutic ion release

The pH values of the DMEM/F12-FBS complete cell culture medium after 24 h of treatment with the SBG and PBG materials (at doses of 50 and 5 mg/mL) are displayed in Fig. 3a,b. The SBG materials induced a moderate or slight alkalinisation of the environment, with the pH reaching values in the range of ~8.2–8.8 and ~7.8–8.4 for powder mass/medium volume ratios of ~50 and 5 mg/mL, respectively. This was expected, since the decomposition of silicate glasses is triggered by a diffusion-controlled protons/hydronium – alkali/alkali earth ion exchange, with the silicate glass network believed to start breaking down only at a pH higher than 8 – 9 [63,74]. In contrast, the PBG materials with CuO and/or Ga_2O_3 acidified the biological testing medium (more marked for Ga-containing PBGs at high dose), rendering pH values into a broader (~6.5–7) or narrower (~7.1–7.2) range when used at doses of 50 and 5 mg/mL, respectively. The acidification of the medium is owned to the degradation mechanism of phosphate glasses, based on the hydrolysis of phosphate network by the nucleophilic attack of water, which leads to the scission of the P–O–P bonds, and release of (mostly) metaphosphate rings [75,76]. Furthermore, the presence of metallic cations (withdrawing electron density from P–O bonds) is known to act as a catalytic agent for the decomposition of phosphate glasses. A particular situation was met for the parent (PBG-C0G0) and PBG-C5G0 formulations, which have led low modifications of the medium pH (*i.e.*, ~7.0–7.2), irrespective of powder dose (50 or 5 mg/mL). This can be linked to the unaltered iron content of these two types of PBGs. Iron possesses a high field strength which leads to an increased glass network durability [75].

The concentrations of ions (Cu and Ga) with potential therapeutic effect released by the SBG and PBG materials in the DMEM/F12-FBS complete culture medium after 24 h of incubation were assessed by ICP-MS, and are given in Figs. 3c–f. It was observed that the concentration level of Cu and Ga ions released in the biological environment is dependent on their corresponding amounts incorporated in the glass SBG and PBG structure. Interestingly, Cu ions were released in similar concentrations for both SBGs and PBGs (*i.e.*, ~50–110 and 10–36 mg/mL and powder doses of 50 and 5 mg/mL, respectively). However, Ga ions were leached by the SBG materials at concentrations of 1–2 orders of magnitude lower with respect to PBGs (*i.e.*, ~0.2–6 *vs.* 9–135 mg/L). This hinted that Ga ions form stronger chemical bonds (are part of more durable structural arrangements) in SBGs, suggesting a predominantly network former role of Ga in SBGs. Ga ions

could have a coordination number of 4, and therefore are able to form tetrahedral structural units $(GaO_4)^{2-}$ in SBGs. Nevertheless, only scarce evidence of this theory could be found. The negative charge of the $(GaO_4)^{2-}$ units can be compensated by the delocalization of network modifying ions [36,77].

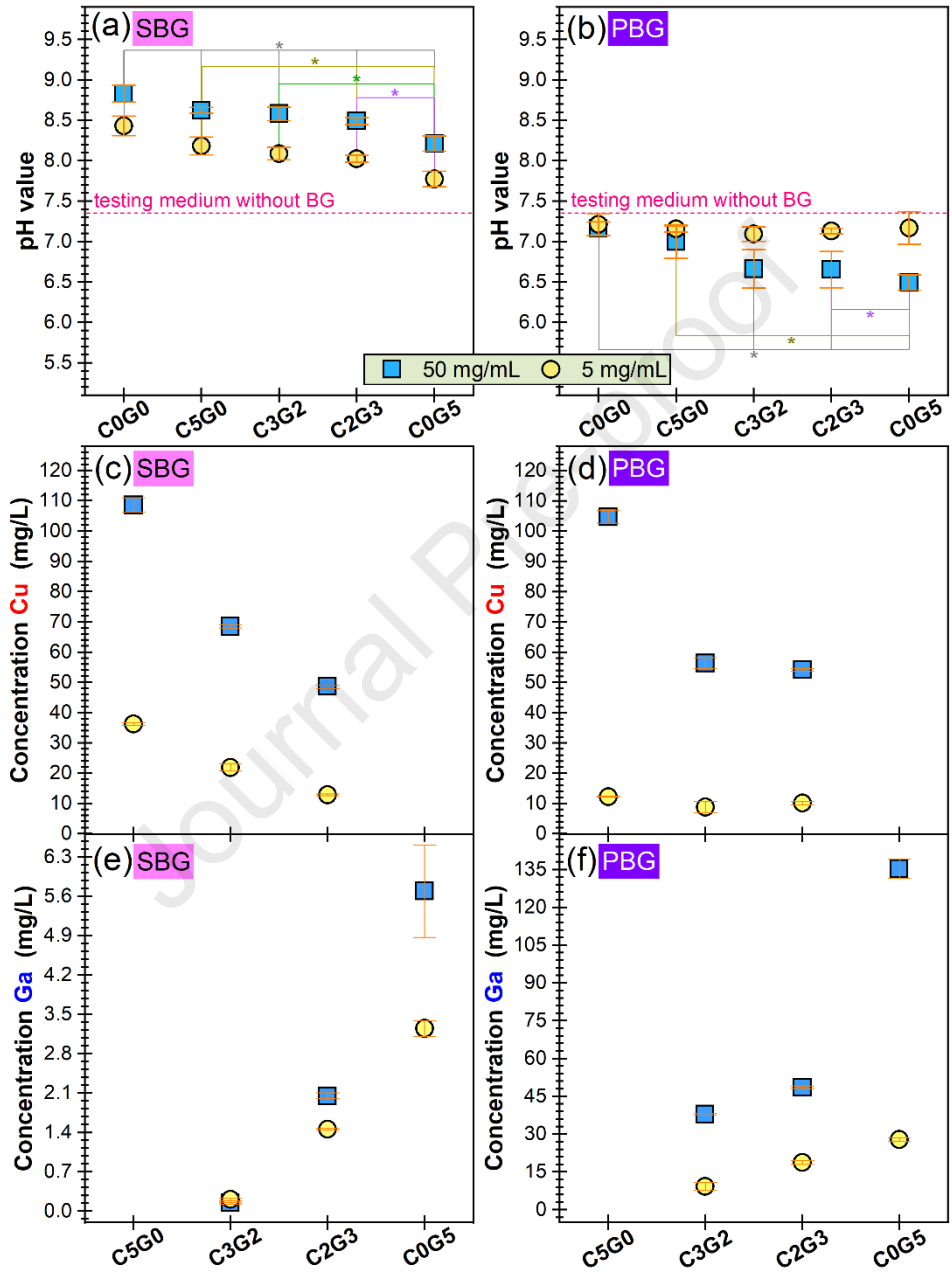

Figure 3: *The evolution of the pH values of the complete cell culture medium after 24 h in presence of doses of 50 and 5 mg/mL of (**a**) SBG and (**b**) PBG powders. The concentrations of (**c**,**d**) Cu and (**e**,**f**) Ga therapeutic ions released by (**a**,**c**) SBGs and (**b**,**d**) PBGs (tested at doses of 50 and 5 mg/mL) after immersion in the complete cell culture medium for 24 h, as determined by ICP-MS.*

3.2.2 Cytocompatibility assays

The cell viability/proliferation and death results, recorded at glass concentrations of 50 and 5 mg/mL, are comparatively displayed in Fig. 4a–d. The correlation of the MTS and LDH results indicated that only a concentration of 50 mg/mL of SBG-C0G5 provided cell viability comparable to the control (Fig. 4a,b), but induced an increase in cell death (Fig. 4c). At this concentration the other compositional systems were cytotoxic. This was caused by the release of Cu ions from SBGs and PBGs into the culture medium at high concentrations of ~50–110 mg/L, situated above the cytotoxicity limit of Cu (*i.e.*, ~10 mg/L) recently reported by Wang *et al.* for the SBG SiO_2–CaO–P_2O_5–CuO system [78]. The release of Ga ions (stronger – 135–150 mg/L – in the case of PBG-C0G5), decreased cell viability to a value of ~75–80%, which was still considered unacceptable after only 24 h.

Subsequently, a decreased concentration (*i.e.*, 5 mg/mL) of SBG and PBG in the culture medium was trialled, to achieve a lower therapeutic ion release rate. Consequently, the MTS tests showed that neither SBGs nor PBGs were detrimental towards cell viability, which was situated above 92% for all tested samples (Fig. 4a,b). The LDH release was not increased at this powder-to-medium concentration (Fig. 4c,d). Correlating these results with those of cell viability/proliferation, it can be concluded that SBG and PBG materials had no cytotoxic effect when used at doses of 5 mg/mL.

3.2.3 Antibacterial tests

All SBG and PBG compositional systems were further evaluated in terms of antimicrobial efficacy against one of the most aggressive and widespread pathogens, *S. aureus*, which is responsible for a wide range of clinical infections [79]. The antimicrobial potential of SBG and PBG materials (at doses of 5 mg/mL) was evaluated using suspensions of *S. aureus* in liquid culture medium (*i.e.*, nutrient broth). The antibacterial activity bar-charts are shown in Fig. 4e,f. For the control sample (*i.e.*, culture medium inoculated with 10^5 CFU/mL *S. aureus*), the bacterial cells developed well, reaching a CFU value with ~4 orders of magnitude higher than the seeded one after 24 h. Interestingly, for SBG powders with CuO and/or Ga_2O_3, a strong antibacterial effect was recorded (more marked for C3G2 and C2G3 glasses). Specifically, ~2-log and ~5-log viable CFUs reductions were observed with respect to the seeded CFUs number and control sample, respectively. It was thus highlighted that the antibacterial efficiency is accentuated by the

simultaneous release of Cu and Ga ions from the SBG materials, and their synergic action (with emphasis on C2G3). The PBG powders had at best a weak bacteriostatic effect.

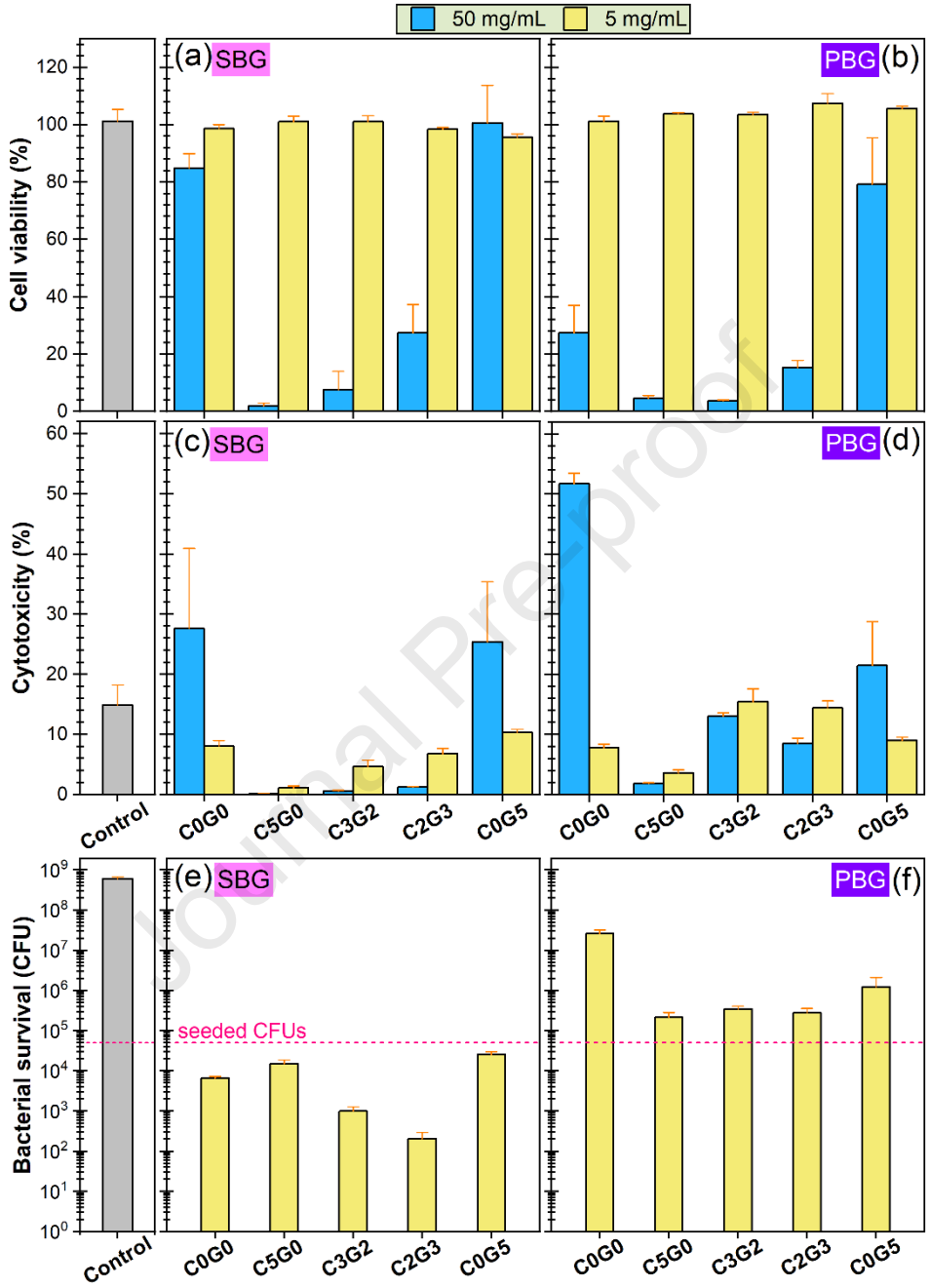

Figure 4: *Bar charts representation of (**a**–**d**) cytocompatibility and (**e**,**f**) antibacterial activity of the SBG and PBG materials. The NIH/3T3 (ATCC® CRL−1658™) mouse fibroblast (**a**,**b**) cell viability/proliferation (evaluated by the MTS assay) and (**c**,**d**) cytotoxicity (inferred by the LDH test) at 24 h of the (**a**,**c**) SBG and (**b**,**d**) PBG materials, at powder mass-to-medium volume ratios of 50 and 5 mg/mL. The antimicrobial activity at 24 h (represented in log-scale) of the (**e**) SBG and (**f**) PBG materials (at powder doses of 5 mg/mL) against the S. aureus bacterial strain.*

4. Discussion

Low connectivity glasses, such as SBGs and PBGs, exhibit intricate networks, with each of chemical constituents possessing a definite structural role, which can vary according to its concentration and lattice site. Network formers (*i.e.*, Si and P) generate a highly cross-linked network of bridging oxygen (BO) bonds and create the building blocks of glasses. BGs can be transformed into a true wonder-materials by customisation of incorporated network modifiers (most often, alkali and alkaline earth metal oxides, *i.e.*, Na_2O, K_2O, CaO and MgO). Network modifiers depolymerise and transform the glass structure by turning the BO atoms with a predominantly covalent chemical bonding character (*e.g.*, Si–O–Si and P–O–P bonds) into non-bridging oxygen (NBO) atoms forming linkages with ionic character (*e.g.*, Si–O–M^+, M^+ = cation modifier). The third category of constituents are the network intermediates which can act either as network formers or modifiers depending on the glass composition and structural location.

Currently, the doping of biocompatible SBGs and PBGs glasses with bioactive potent oxides (*e.g.*, Ag_2O, SrO, ZnO, CeO_2, CuO, Ga_2O_3) is widely considered for tuning and expanding their functionality (with angiogenesis, antioxidant and antimicrobial properties being the most targeted) and applicability range (from hard tissue to soft tissue and wound healing applications) to suit specific biomedical demands [6,11,63]. Since therapeutic agents inserted in the backbone of the glass modify the physical properties of new BGs, it becomes of major importance to unveil their specific structural role (as either *network former*, *modifier or intermediate*)/chemical environment, as this will govern their leaching rate in the biological medium, and thereby the BG effectiveness.

In this work, the structural and preliminary biological effects of Cu and Ga were explored when incorporated solely or concurrently in SBG and PBG systems. If in the case of Cu, the scientific literature rather consensually agrees on its network modifier role [31,80], in the case of Ga, the evidences are rather infrequent and indecisive. In a SBG structure, Ga^{3+} ions are believed to exhibit a transitional behaviour between network formers and network modifiers [36]. Furthermore, studies of both Ga-substituted SBGs and PBGs have indicated that the release of Ga^{3+} in physiological media is not directly proportional to its concentration in the glass, but is rather dependent on its location in the vitreous network [34,36]. Sanchez-Salcedo *et al.* [36] concluded that in mesoporous SBGs, Ga^{3+} acts as a network modifier in the highly polymerized

regions (*i.e.*, regions with bridging oxygen predominance) and as a network former in the regions with non-bridging oxygen prevalence.

The thermal analyses (*showing that Cu incorporation decreased the T_g of both SBGs and PBGs, whilst Ga augmented and reduced the T_g of SBGs and PBGs, respectively*), XPS measurements (*indicating that Cu chemical state is similar in both SBG and PBG materials, whilst Ga is in a richer chemical environment in PBG with respect to SBG*) and the ion-release quantifications (*unveiling that Cu is released in similar concentrations for SBGs and PBGs, whilst Ga is leached by PBGs in concentrations with 1–2 orders of magnitude higher than the SBGs*) suggested that Ga plays dissimilar structural roles in silica- and phosphate-based glasses. Since the elucidation of the structural role of Ga could be of high significance for the biomedical predictability of such derived glasses and for the future applications to be developed, further experimental investigations have been carried out *via* EXAFS spectroscopy. EXAFS is a powerful tool for structural characterisation, enabling the independent determination of the local structure around each atomic species in a material (element selectivity), regardless its complexity. Another specific advantage of this technique is the use of the same mathematical formalism in approaching highly disordered materials, such as amorphous or glasses, and periodical crystalline solids. EXAFS defines the oscillations of the X-ray absorption spectra above an absorption edge, which denotes the sudden increase of the absorption coefficient whenever the energy of the incident X-ray photons equals the binding energy of the inner electrons of the absorbing species. Consequently, these edges are known as K or $L_{1\text{-}3}$, depending on the electron core-level ($1s_{1/2}$, $2s_{1/2}$, $2p_{1/2,}$ $2p_{3/2}$) on which the photo absorption took place. For this purpose, two Cu and Ga substituted glasses were selected, namely the SBG-C2G3 and PBG-C2G3 ones.

The Ga K-edge absorption spectra of the SBG- and PBG-C2G3 glasses are shown in Fig. 5a. As observed, the EXAFS oscillations have a simple periodicity, without split or complex-shape maxima, which would result from the superposition of more frequencies. This suggests a dominant contribution to EXAFS from a unique neighbouring shell of Ga, *i.e.* the nearest oxygen neighbours. Also, the oscillation frequency in the spectrum of PBG-C2G3 is slightly larger than that in the SBG-C2G3 spectrum, pointing to a larger Ga–O distance in the structure of the former. These qualitative observations were confirmed by further EXAFS analysis.

The k^3-weighted EXAFS spectra and their Fourier transforms (FT) are shown in Fig. 5b,c. The main maximum of FT's corresponds to the nearest oxygen neighbours of Ga. The advanced

structural disorder of the higher-order neighbouring shells drastically reduces their contributions to FT. The main maximum of FT was isolated, backtransformed into *k*-space and non-linearly fitted with the oxygen surrounding. The results of the fit (Table 2) indicate the four-fold coordination of Ga in SBG-C2G3 glass and six-fold coordination in PBG-C2G3, *revealing that Ga acts as network former in SBG and as network modifier in PBG*. The mean-square fluctuation of the Ga–O distance (σ^2), measuring the structural disorder of the short-range environment of Ga, is three times larger in the PBG glass with respect to SBG, indicating much more ordered GaO_4 tetrahedra in the SBG structure than the GaO_6 octahedra in PBG. This is related to the Ga configuration in the two glasses. The Ga incorporation in the silicate network, in the former case, preserves the structural order of the SiO_4 units, whereas the network-modifier Ga in PBG, placed outside the PO_4 cages and with the Ga–O distance ranging in a broad interval, has a more disordered oxygen surrounding. This explains the smaller amplitude of the main maximum in the PBG FT, by comparison with the SBG glass (Fig. 5c), despite the larger number of oxygen neighbours of Ga in the PBG structure.

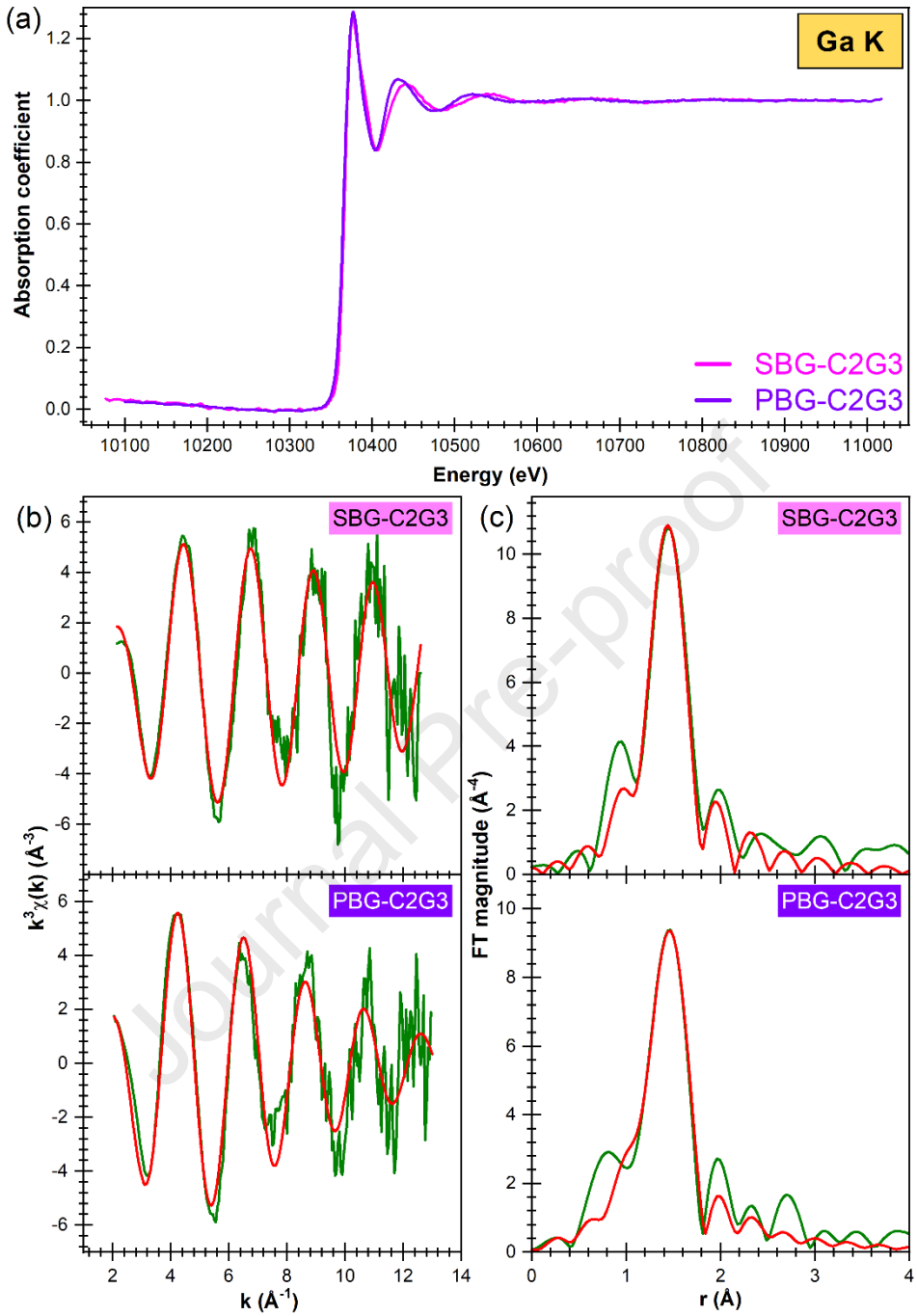

Figure 5: *(**a**) Normalized absorption spectra of the SBG-C2G3 and PBG-C2G3 materials, measured at the Ga K edge. (**b**,**c**) Ga K-edge EXAFS of the SBG-C2G3 and PBG-C2G3: (**b**) k^3-weighted EXAFS spectra and (**c**) the magnitude of their Fourier transforms. The raw data and their fit with the nearest oxygen neighbours were shown by green and red lines, respectively.*

Table 2: *Nearest oxygen surrounding of Ga, as inferred by EXAFS: coordination numbers (N_O), interatomic Ga–O distances (R), and their mean-square fluctuations (σ^2) around average values.*

Sample code	N_O	R (Å)	$\sigma^2 \times 10^3$ (Å^2)	Ga structural role
SBG-C2G3	4.0±0.2	1.831±0.006	2.1±0.7	Network former

PBG-C2G3	5.8±0.3	1.876±0.007	6±1	Network modifier

As emphasized in the Introduction, Cu and Ga have different antibacterial mechanisms with the former relying on the generation of ROS species and denaturation of DNA/RNA by ion chelation, and the latter on the disruption of ion metabolism. This could account for their efficacy when coupled in the SBG (*i.e.*, C3G2 and C2G3 series), hindering the bacterial development by a 1–2 orders of magnitude with respect to the single Cu or Ga substituted glasses. It is to be noted that the XPS measurements revealed that a significant part of the original Cu^{2+} (in the precursor) was reduced to Cu^{1+} oxidation state (in both the SBG and PBG glasses). This was facilitated by the lower Gibbs free energy of oxidation of Cu_2O, and thereby, its superior thermodynamic driving force for formation with respect to CuO [81]. However, this could work to the benefit of these bioactive glasses, since it was noticed that Cu^{1+} ions are more toxic towards bacteria than Cu^{2+} ions under test conditions that simulate microbial contamination [32].

The significantly higher antibacterial efficacy of SBGs compared to PBGs might be linked with the augmentation of copper's effect in aerobic bacteria cells due to pH changes. Specifically, Cu is an essential element used by many enzymes and processes involved in bacterial metabolism, having its own transporters. Cu^{1+} enters with much ease by diffusion in bacterial cells, with respect to Cu^{2+}. An alkaline environment is known to favour the ionization of Cu in the form of Cu^{1+} rather than Cu^{2+}, leading to Cu^{1+} accumulation in the cytoplasm of the bacteria, with toxic effects on enzymes and DNA [82–85]. PBGs that generate an acidic environment will hinder the massive Cu intake having thus a lesser bacterial toxicity. Also, Cu ions bind to cell plasma molecules and lead to local destruction by a mechanism of formation of hydroperoxide radicals, that have a greater effect in alkaline environments rather than media with pH values in the range of 6–7 that occur in the case of PBGs [86]. Furthermore, cytochrome c oxidase, a respiratory membrane bound enzyme in many bacteria and mitochondria that contains two Cu catalytic sites, is known to exhibit a ten-fold reduction in activity at higher pH 8.5–9 than at pH 7 [87]. This reduction is not due to protein misfolding, but rather to heme a3-CuB catalytic centre impairment in exercising its function [87]. In an alkaline medium Ga tends to produce $Ga(OH)^{4-}$ species which deepen the deleterious effect on bacterial cells [88]. Cumulatively, these small "nudges" on bacterial cell metabolism overcomes their ability to adapt, leading to cell death rather than cell proliferation arrest.

5. Conclusions

The interlinked structural and (preliminary) biological effects induced by the Cu and/or Ga incorporation into silica- and phosphate-based bioactive glasses was explored for the first time. EXAFS spectroscopy indicated the clear distinction between the four- and six-fold oxygen coordination of Ga, pointing out its network former or modifier configuration. The FTIR, X-ray photoelectron and EXAFS spectroscopies indicated that Cu acted as network modifier irrespective of type of glass, whilst Ga had a prominent glass network former role in SBGs, and network modifier role in PBGs. Consequently, the SBGs and PBGs fostered different ion leaching patterns, with Cu ions being released in similar concentrations (ranging from 10–35 ppm and 50–110 ppm at BG doses of 5 and 50 mg/mL, respectively) for both type of glasses, and the Ga ions being released 1–2 orders of magnitude lower in the case of SBGs (*i.e.*, 0.2–6 ppm) compared to PBGs (*i.e.*, 9–135 ppm). No cytotoxic effects were found at a dose of 5 mg/mL of bioactive glass powder in cell culture medium. At this concentration the antimicrobial efficiency was augmented by the coupled release of Cu and Ga ions from SBG. The most promising candidate material was delineated as the $38.5SiO_2$—$34.1CaO$—$5.6P_2O_5$—$16.2MgO$—$0.6CaF_2$—$2.0CuO$—$3.0Ga_2O_3$ (mol%) formulation, which led to a moderate Cu and Ga ion release, excellent cytocompatibility and noteworthy antibacterial efficacy against *S. aureus*.

The improved antibacterial efficiency, by the co-addition of Cu and Ga to silica-based bioactive glasses, might enable the future development of solutions to mitigate the increasing number of nosocomial infections and the emergence of antibiotic resistant strains. Impending complex biological studies are envisaged to unravel the antibacterial mechanisms at play and to understand the extent of the antimicrobial range (by testing against a large array of Gram-positive and Gram-negative bacterial strains and fungi), as well as to assess the capability of Cu and Ga to stimulate osteogenesis and angiogenesis.

Acknowledgements

The authors thank for the financial support of the Romanian National Authority for Scientific Research and Innovation (CNCS-UEFISCDI) in the framework of PN-III-P1-1.1-TE-2016-1501 and PN-III-P1-1.1-TE-2019-0463 projects, and to the institutional Core Program 21N. This work was also developed within the scope of the project CICECO-Aveiro Institute of Materials, FCT

Ref. UID/CTM/50011/2019, financed by national funds through the FCT/MCTES. The partial support of the Engineering and Physical Sciences Research Council [grant number EP/K029592/1] via the Centre for Innovative Manufacturing in Medical Devices (MeDe Innovation) is recognized. The authors are thankful to Dr. C.C. Negrila for performing the XPS analyses, and to Dr. G. Popescu-Pelin for carrying out part of the EDXS measurements.

References

[1] E. Zhang, X. Zhao, J. Hu, R. Wang, S. Fu, G. Qin, Bioactive Materials. 6 (2021) 2569–2612. https://doi.org/10.1016/j.bioactmat.2021.01.030.

[2] J. Jiao, S. Zhang, X. Qu, B. Yue, Frontiers in Cellular and Infection Microbiology. 11 (2021) 611. https://doi.org/10.3389/fcimb.2021.693939.

[3] D.T. Elliott, R.J. Wiggins, R. Dua, Journal of Biomedical Materials Research Part B: Applied Biomaterials. 109 (2021) 973–981. https://doi.org/10.1002/jbm.b.34762.

[4] B.W. Stuart, G.E. Stan, A.C. Popa, M.J. Carrington, I. Zgura, M. Necsulescu, D.M. Grant, Bioactive Materials. 8 (2022) 325–340. https://doi.org/10.1016/j.bioactmat.2021.05.055.

[5] G. Brunello, H. Elsayed, L. Biasetto, Materials. 12 (2019) 2929. https://doi.org/10.3390/ma12182929.

[6] H.R. Fernandes, A. Gaddam, A. Rebelo, D. Brazete, G.E. Stan, J.M.F. Ferreira, Materials. 11 (2018) 2530. https://doi.org/10.3390/ma11122530.

[7] J.M.F. Ferreira, Biomedical Journal of Scientific & Technical Research. 1 (2017) 936–939. https://doi.org/10.26717/BJSTR.2017.01.000335.

[8] I. Cacciotti, Journal of Materials Science. 52 (2017) 8812–8831. https://doi.org/10.1007/s10853-017-1010-0.

[9] L.L. Hench, Journal of Materials Science: Materials in Medicine. 17 (2006) 967–978. https://doi.org/10.1007/s10856-006-0432-z.

[10] J.D. Musgraves, J. Hu, L. Calvez, Springer Handbook of Glass, Springer International Publishing, Berlin, 2019. https://doi.org/10.1007/978-3-319-93728-1.

[11] F. Baino, S. Hamzehlou, S. Kargozar, Journal of Functional Biomaterials. 9 (2018) 25. https://doi.org/10.3390/jfb9010025.

[12] A. Goel, S. Kapoor, R.R. Rajagopal, M.J. Pascual, H.-W. Kim, J.M.F. Ferreira, Acta Biomaterialia. 8 (2012) 361–372. https://doi.org/https://doi.org/10.1016/j.actbio.2011.08.026.

[13] A. Goel, S. Kapoor, A. Tilocca, R.R. Rajagopal, J.M.F. Ferreira, Journal of Materials Chemistry B. 1 (2013) 3073. https://doi.org/10.1039/c3tb20163e.

[14] A.C. Popa, H.R. Fernandes, M. Necsulescu, C. Luculescu, M. Cioangher, V. Dumitru, B.W. Stuart, D.M. Grant, J.M.F. Ferreira, G.E. Stan, Ceramics International. 45 (2019) 4368–4380. https://doi.org/10.1016/j.ceramint.2018.11.112.

[15] F.E. Ciraldo, E. Boccardi, V. Melli, F. Westhauser, A.R. Boccaccini, Acta Biomaterialia. 75 (2018) 3–10. https://doi.org/https://doi.org/10.1016/j.actbio.2018.05.019.

[16] T. Tite, A.C. Popa, I.M. Chirica, B.W. Stuart, A.C. Galca, L.M. Balescu, G. Popescu-Pelin, D.M. Grant, J.M.F. Ferreira, G.E. Stan, Applied Surface Science. 541 (2021) 148640. https://doi.org/10.1016/j.apsusc.2020.148640.

[17] D. Gupta, K.M.Z. Hossain, M. Roe, E.F. Smith, I. Ahmed, V. Sottile, D.M. Grant, ACS Applied Bio Materials. 4 (2021) 5987–6004. https://doi.org/10.1021/acsabm.1c00120.

[18] R. Shafaghi, O. Rodriguez, A.W. Wren, L. Chiu, E.H. Schemitsch, P. Zalzal, S.D. Waldman, M. Papini, M.R. Towler, Journal of Biomedical Materials Research Part A. 109 (2021) 146–158. https://doi.org/10.1002/jbm.a.37012.

[19] K. Schuhladen, L. Stich, J. Schmidt, A. Steinkasserer, A.R. Boccaccini, E. Zinser, Biomaterials Science. 8 (2020) 2143–2155. https://doi.org/10.1039/C9BM01691K.

[20] W.C. Lepry, S.N. Nazhat, Materials Advances. 1 (2020) 1371–1381. https://doi.org/10.1039/D0MA00360C.

[21] G.E. Stan, T. Tite, A.-C. Popa, I.M. Chirica, C.C. Negrila, C. Besleaga, I. Zgura, A.C. Sergentu, G. Popescu-Pelin, D. Cristea, L.E. Ionescu, M. Necsulescu, H.R. Fernandes, J.M.F. Ferreira, Coatings. 10 (2020) 1119. https://doi.org/10.3390/coatings10111119.

[22] R. Sergi, D. Bellucci, V. Cannillo, Coatings. 10 (2020) 757. https://doi.org/10.3390/coatings10080757.

[23] D.S. Brauer, Angewandte Chemie International Edition. 54 (2015) 4160–4181. https://doi.org/10.1002/anie.201405310.

[24] J.C. Knowles, Journal of Materials Chemistry. 13 (2003) 2395. https://doi.org/10.1039/b307119g.

[25] I. Ahmed, M. Lewis, I. Olsen, J.C. Knowles, Biomaterials. 25 (2004) 491–499. https://doi.org/10.1016/S0142-9612(03)00546-5.

[26] M. Al Qaysi, A. Petrie, R. Shah, J.C. Knowles, Journal of Materials Science: Materials in Medicine. 27 (2016) 157. https://doi.org/10.1007/s10856-016-5770-x.

[27] B.W. Stuart, M. Gimeno-Fabra, J. Segal, I. Ahmed, D.M. Grant, Applied Surface Science. 416 (2017) 605–617. https://doi.org/10.1016/j.apsusc.2017.04.110.

[28] S. Kaya, M. Cresswell, A.R. Boccaccini, Materials Science and Engineering: C. 83 (2018) 99–107. https://doi.org/10.1016/j.msec.2017.11.003.

[29] L. Drago, M. Toscano, M. Bottagisio, Materials. 11 (2018) 326. https://doi.org/10.3390/ma11020326.

[30] Y. Liu, N. Nie, H. Tang, C. Zhang, K. Chen, W. Wang, J. Liu, ACS Applied Materials & Interfaces. 13 (2021) 11631–11645. https://doi.org/10.1021/acsami.0c22746.

[31] F. Baino, Bioengineering. 7 (2020) 45. https://doi.org/10.3390/bioengineering7020045.

[32] T.M. Gross, J. Lahiri, A. Golas, J. Luo, F. Verrier, J.L. Kurzejewski, D.E. Baker, J. Wang, P.F. Novak, M.J. Snyder, Nature Communications. 10 (2019) 1979. https://doi.org/10.1038/s41467-019-09946-9.

[33] United States Environmental Protection Agency. Test method for efficacy of copper alloy surfaces as a sanitizer (Washington DC, 2008), (n.d.). https://archive.epa.gov/pesticides/oppad001/web/pdf/copper-copper-alloy-surface-protocol.pdf (accessed December 23, 2021).

[34] S.P. Valappil, D. Ready, E.A.A. Neel, D.M. Pickup, W. Chrzanowski, L.A. O'Dell, R.J. Newport, M.E. Smith, M. Wilson, J.C. Knowles, Advanced Functional Materials. 18 (2008) 732–741. https://doi.org/10.1002/adfm.200700931.

[35] A. Łapa, M. Cresswell, I. Campbell, P. Jackson, W.H. Goldmann, R. Detsch, A.R. Boccaccini, Advanced Engineering Materials. 22 (2020) 1901577. https://doi.org/10.1002/adem.201901577.

[36] S. Sanchez-Salcedo, G. Malavasi, A. Salinas, G. Lusvardi, L. Rigamonti, L. Menabue, M. Vallet-Regi, Materials. 11 (2018) 367. https://doi.org/10.3390/ma11030367.

[37] O. Olakanmi, J.S. Gunn, S. Su, S. Soni, D.J. Hassett, B.E. Britigan, Antimicrobial Agents and Chemotherapy. 54 (2010) 244–253. https://doi.org/10.1128/AAC.00655-09.

[38] S. Pourshahrestani, E. Zeimaran, N. Adib Kadri, N. Gargiulo, S. Samuel, S.V. Naveen, T. Kamarul, M.R. Towler, Journal of Materials Chemistry B. 4 (2016) 71–86. https://doi.org/10.1039/C5TB02062J.

[39] C.A. Dascălu, A. Maidaniuc, A.M. Pandele, S.I. Voicu, T. Machedon-Pisu, G.E. Stan, A. Cîmpean, V. Mitran, I.V. Antoniac, F. Miculescu, Applied Surface Science. 494 (2019) 335–352. https://doi.org/10.1016/j.apsusc.2019.07.098.

[40] F. Kurtuldu, N. Mutlu, M. Michálek, K. Zheng, M. Masar, L. Liverani, S. Chen, D. Galusek, A.R. Boccaccini, Materials Science and Engineering: C. 124 (2021) 112050. https://doi.org/10.1016/j.msec.2021.112050.

[41] S. Kapoor, A. Goel, A. Tilocca, V. Dhuna, G. Bhatia, K. Dhuna, J.M.F. Ferreira, Acta Biomaterialia. 10 (2014) 3264–3278. https://doi.org/https://doi.org/10.1016/j.actbio.2014.03.033.

[42] A. Nawaz, S. Bano, M. Yasir, A. Wadood, M.A. Ur Rehman, Materials Advances. 1 (2020) 1273–1284. https://doi.org/10.1039/D0MA00325E.

[43] C.Y.K. Lung, M.M. Abdalla, C.H. Chu, I. Yin, S.-R. Got, J.P. Matinlinna, Materials. 14 (2021) 961. https://doi.org/10.3390/ma14040961.

[44] P.P. Cortez, A.F. Brito, S. Kapoor, A.F. Correia, L.M. Atayde, P. Dias-Pereira, A.C. Maurício, A. Afonso, A. Goel, J.M.F. Ferreira, Journal of Biomedical Materials Research Part B: Applied Biomaterials. 105 (2017) 30–38. https://doi.org/10.1002/jbm.b.33529.

[45] M. Schumacher, P. Habibovic, S. van Rijt, Bioactive Materials. 6 (2021) 1921–1931. https://doi.org/10.1016/j.bioactmat.2020.12.007.

[46] M. Kuwik, J. Pisarska, W.A. Pisarski, Materials. 13 (2020) 4746. https://doi.org/10.3390/ma13214746.

[47] S.J. Watts, R.G. Hill, M.D. O'Donnell, R.V. Law, Journal of Non-Crystalline Solids. 356 (2010) 517–524. https://doi.org/10.1016/j.jnoncrysol.2009.04.074.

[48] P. Goj, A. Wajda, A. Stoch, I. Krakowiak, P. Stoch, Materials. 14 (2021) 2065. https://doi.org/10.3390/ma14082065.

[49] T. Taguchi, J. Harada, A. Kiku, K. Tohji, K. Shinoda, Journal of Synchrotron Radiation. 8 (2001) 363–365. https://doi.org/10.1107/S0909049500018458.

[50] T. Taguchi, Q. Xiao, J. Harada, Journal of Synchrotron Radiation. 6 (1999) 170–171. https://doi.org/10.1107/S0909049599000084.

[51] B. Ravel, M. Newville, Journal of Synchrotron Radiation. 12 (2005) 537–541. https://doi.org/10.1107/S0909049505012719.

[52] B. Ravel, Journal of Synchrotron Radiation. 8 (2001) 314–316. https://doi.org/10.1107/S090904950001493X.

[53] J.J. Rehr, J. Mustre de Leon, S.I. Zabinsky, R.C. Albers, Journal of the American Chemical Society. 113 (1991) 5135–5140. https://doi.org/10.1021/ja00014a001.

[54] S.I. Zabinsky, J.J. Rehr, A. Ankudinov, R.C. Albers, M.J. Eller, Physical Review B. 52 (1995) 2995–3009. https://doi.org/10.1103/PhysRevB.52.2995.

[55] M. Newville, Journal of Synchrotron Radiation. 8 (2001) 322–324. https://doi.org/10.1107/S0909049500016964.

[56] D. Rohanová, A.R. Boccaccini, D. Horkavcová, P. Bozděchová, P. Bezdička, M. Častorálová, J. Mater. Chem. B. 2 (2014) 5068–5076. https://doi.org/10.1039/C4TB00187G.

[57] F.A. Shah, D.S. Brauer, R.M. Wilson, R.G. Hill, K.A. Hing, Journal of Biomedical Materials Research Part A. 102 (2014) 647–654. https://doi.org/10.1002/jbm.a.34724.

[58] A.C. Popa, G.E. Stan, M.A. Husanu, I. Mercioniu, L.F. Santos, H.R. Fernandes, J.M.F. Ferreira, International Journal of Nanomedicine. 12 (2017) 683–707. https://doi.org/10.2147/IJN.S123236.

[59] M. Mozafari, S. Banijamali, F. Baino, S. Kargozar, R.G. Hill, Acta Biomaterialia. 91 (2019) 35–47. https://doi.org/10.1016/j.actbio.2019.04.039.

[60] International Organization for Standardization, ISO 22309:2011 Microbeam analysis — Quantitative analysis using energy-dispersive spectrometry (EDS) for elements with an atomic number of 11 (Na) or above, Geneva, Switzerland. (2011).

[61] S. Kapoor, A. Goel, M.J. Pascual, J.M.F. Ferreira, Journal of Non-Crystalline Solids. 375 (2013) 74–82. https://doi.org/10.1016/j.jnoncrysol.2013.05.007.

[62] J. Will, L.-C. Gerhardt, A.R. Boccaccini, Adv. Biochem. Eng. Biotechnol. 126 (2012) 195–226. https://doi.org/10.1007/10_2011_106.

[63] J.R. Jones, Acta Biomaterialia. 9 (2013) 4457–4486. https://doi.org/10.1016/j.actbio.2012.08.023.

[64] E.C. Ziemath, M.A. Aegerter, Journal of Materials Research. 9 (1994) 216–225. https://doi.org/10.1557/JMR.1994.0216.

[65] S. Agathopoulos, D.U. Tulyaganov, J.M.G. Ventura, S. Kannan, M.A. Karakassides, J.M.F. Ferreira, Biomaterials. 27 (2006) 1832–1840. https://doi.org/10.1016/j.biomaterials.2005.10.033.

[66] A. Gaddam, A.R. Allu, H.R. Fernandes, G.E. Stan, C.C. Negrila, A.P. Jamale, F.O. Méar, L. Montagne, J.M.F. Ferreira, Journal of the American Ceramic Society. 104 (2021) 2495–2505. https://doi.org/10.1111/jace.17671.

[67] G. le Saoût, P. Simon, F. Fayon, A. Blin, Y. Vaills, Journal of Raman Spectroscopy. 33 (2002) 740–746. https://doi.org/10.1002/jrs.911.

[68] R. Ciceo Lucacel, A.O. Hulpus, V. Simon, I. Ardelean, Journal of Non-Crystalline Solids. 355 (2009) 425–429. https://doi.org/10.1016/j.jnoncrysol.2008.12.012.

[69] B.W. Stuart, C.A. Grant, G.E. Stan, A.C. Popa, J.J. Titman, D.M. Grant, Journal of the Mechanical Behavior of Biomedical Materials. 82 (2018) 371–382. https://doi.org/10.1016/j.jmbbm.2018.03.041.

[70] A.K. Yadav, P. Singh, RSC Advances. 5 (2015) 67583–67609. https://doi.org/10.1039/C5RA13043C.

[71] XPS Interpretation of Copper, (n.d.). https://xpssimplified.com/elements/copper.php (accessed December 23, 2021).

[72] J.F. Moulder, W.F. Stickle, P.E. Sobol, K.D. Bomben, Handbook of X-ray photoelectron spectroscopy: a reference book of standard spectra for identification and interpretation of XPS data, Physical Electronics Division, Perkin-Elmer Corporation, Eden Prairie, MN, USA, 1992.

[73] J.L. Bourque, M.C. Biesinger, K.M. Baines, Dalton Transactions. 45 (2016) 7678–7696. https://doi.org/10.1039/C6DT00771F.

[74] T.M. El-Shamy, C.G. Pantano, Nature. 266 (1977) 704–706. https://doi.org/10.1038/266704a0.

[75] D.A. Avila Salazar, P. Bellstedt, A. Miura, Y. Oi, T. Kasuga, D.S. Brauer, Dalton Transactions. 50 (2021) 3966–3978. https://doi.org/10.1039/D0DT03381B.

[76] M. Watanabe, M. Matsuura, T. Yamada, Bulletin of the Chemical Society of Japan. 54 (1981) 738–741. https://doi.org/10.1246/bcsj.54.738.

[77] G. Malavasi, A. Pedone, M.C. Menziani, The Journal of Physical Chemistry B. 117 (2013) 4142–4150. https://doi.org/10.1021/jp400721g.

[78] X. Wang, F. Cheng, J. Liu, J.-H. Smått, D. Gepperth, M. Lastusaari, C. Xu, L. Hupa, Acta Biomaterialia. 46 (2016) 286–298. https://doi.org/10.1016/j.actbio.2016.09.021.

[79] S.Y.C. Tong, J.S. Davis, E. Eichenberger, T.L. Holland, V.G. Fowler, Clinical Microbiology Reviews. 28 (2015) 603–661. https://doi.org/10.1128/CMR.00134-14.

[80] S. Kargozar, M. Mozafari, S. Ghodrat, E. Fiume, F. Baino, Materials Science and Engineering: C. 121 (2021) 111741. https://doi.org/10.1016/j.msec.2020.111741.

[81] T.B. Reed, Free energy of formation of binary compounds: An atlas of charts for high-temperature chemical calculations, MIT Press, Cambridge, MA, USA, 1972.

[82] C. Rensing, G. Grass, FEMS Microbiology Reviews. 27 (2003) 197–213. https://doi.org/10.1016/S0168-6445(03)00049-4.

[83] J. Quintana, L. Novoa-Aponte, J.M. Argüello, Journal of Biological Chemistry. 292 (2017) 15691–15704. https://doi.org/10.1074/jbc.M117.804492.

[84] B. Grey, T.R. Steck, Applied and Environmental Microbiology. 67 (2001) 5325–5327. https://doi.org/10.1128/aem.67.11.5325-5327.2001.

[85] C. Dennison, S. David, J. Lee, Journal of Biological Chemistry. 293 (2018) 4616–4627. https://doi.org/10.1074/jbc.TM117.000180.

[86] H. Lee, H.J. Lee, D.L. Sedlak, C. Lee, Chemosphere. 92 (2013) 652–658. https://doi.org/10.1016/j.chemosphere.2013.01.073.

[87] D. Riegler, L. Shroyer, C. Pokalsky, D. Zaslavsky, R. Gennis, L.J. Prochaska, Biochimica et Biophysica Acta - Bioenergetics. 1706 (2005) 126–133. https://doi.org/10.1016/j.bbabio.2004.10.002.

[88] B. Hacht, Gallium(III) ion hydrolysis under physiological conditions, 372–376. https://doi.org/10.5012/bkcs.2008.29.2.372.

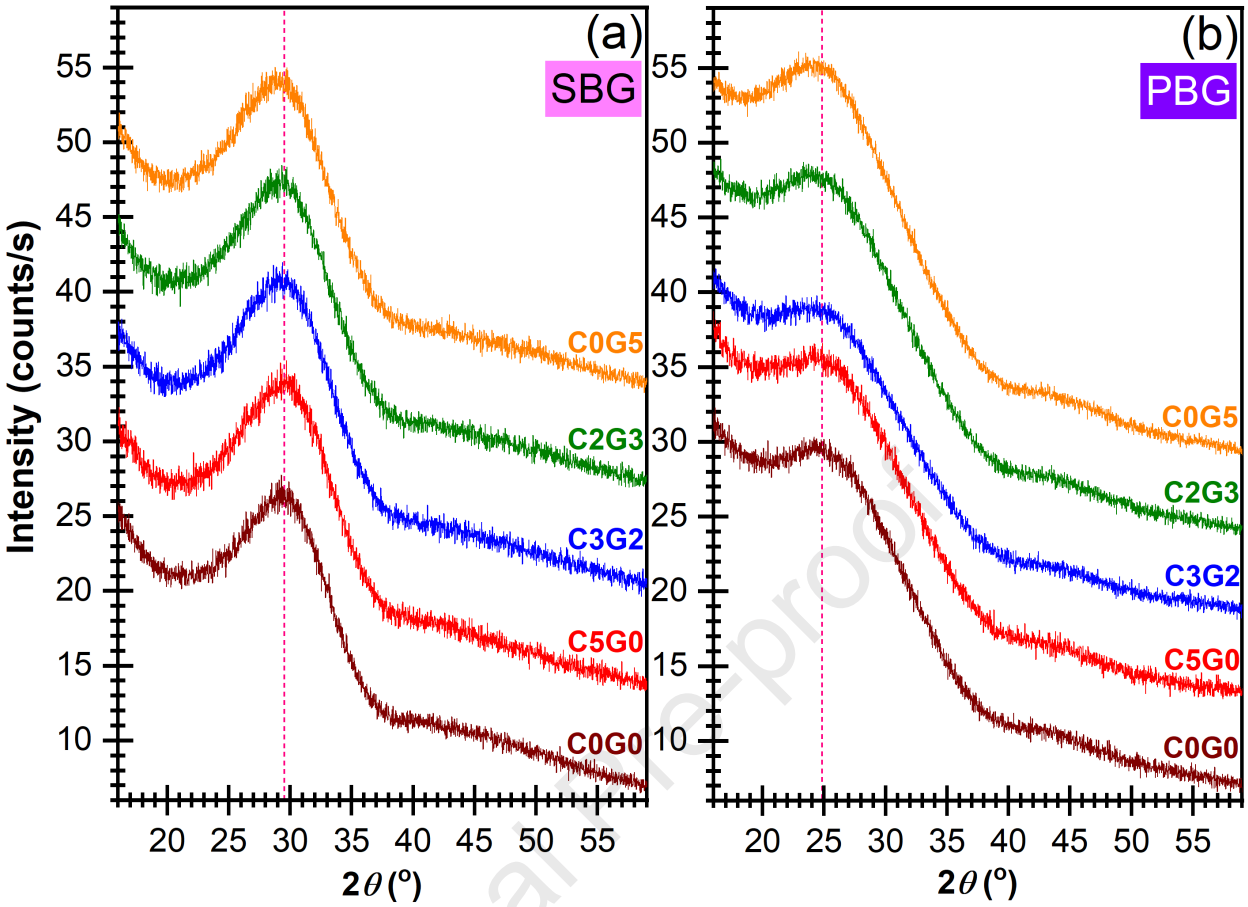

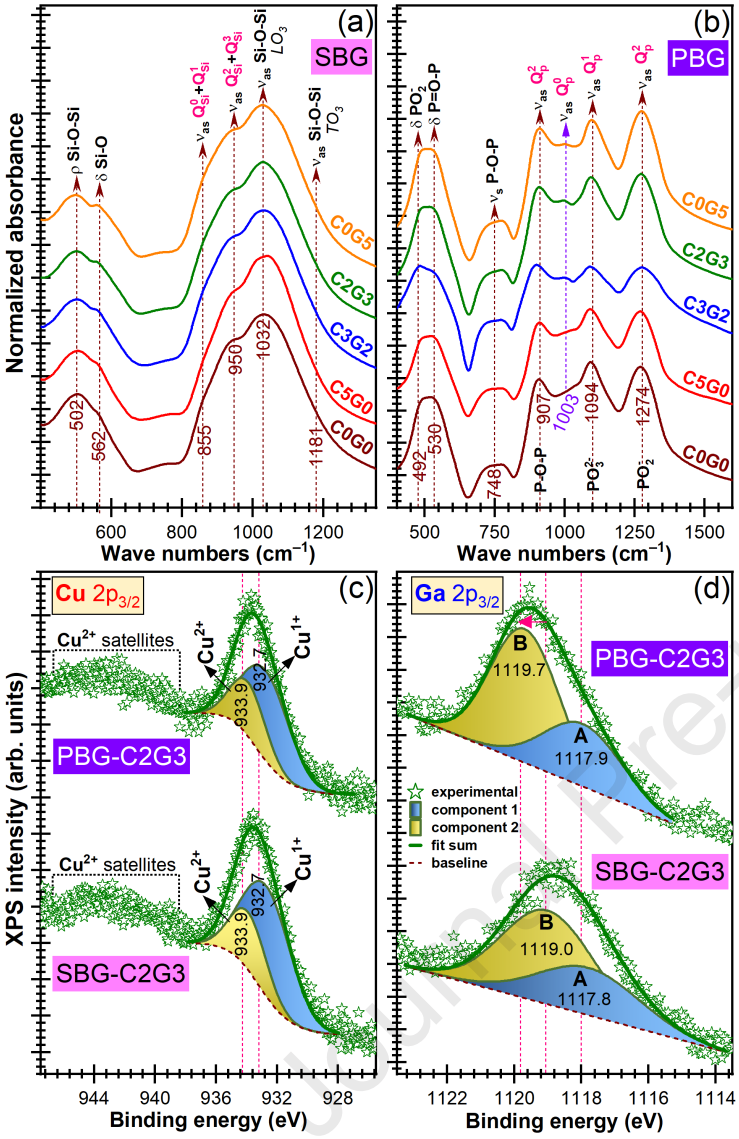

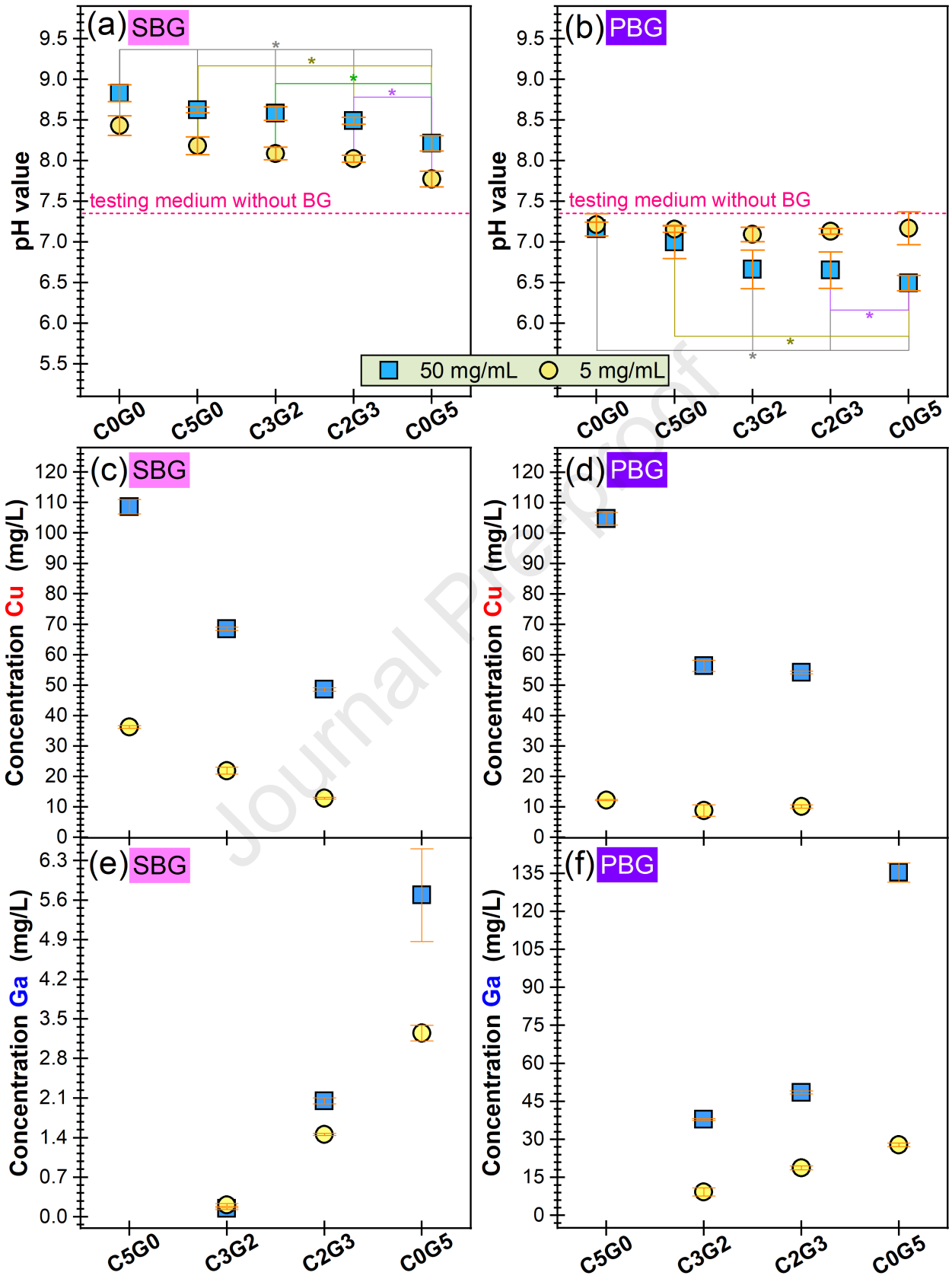

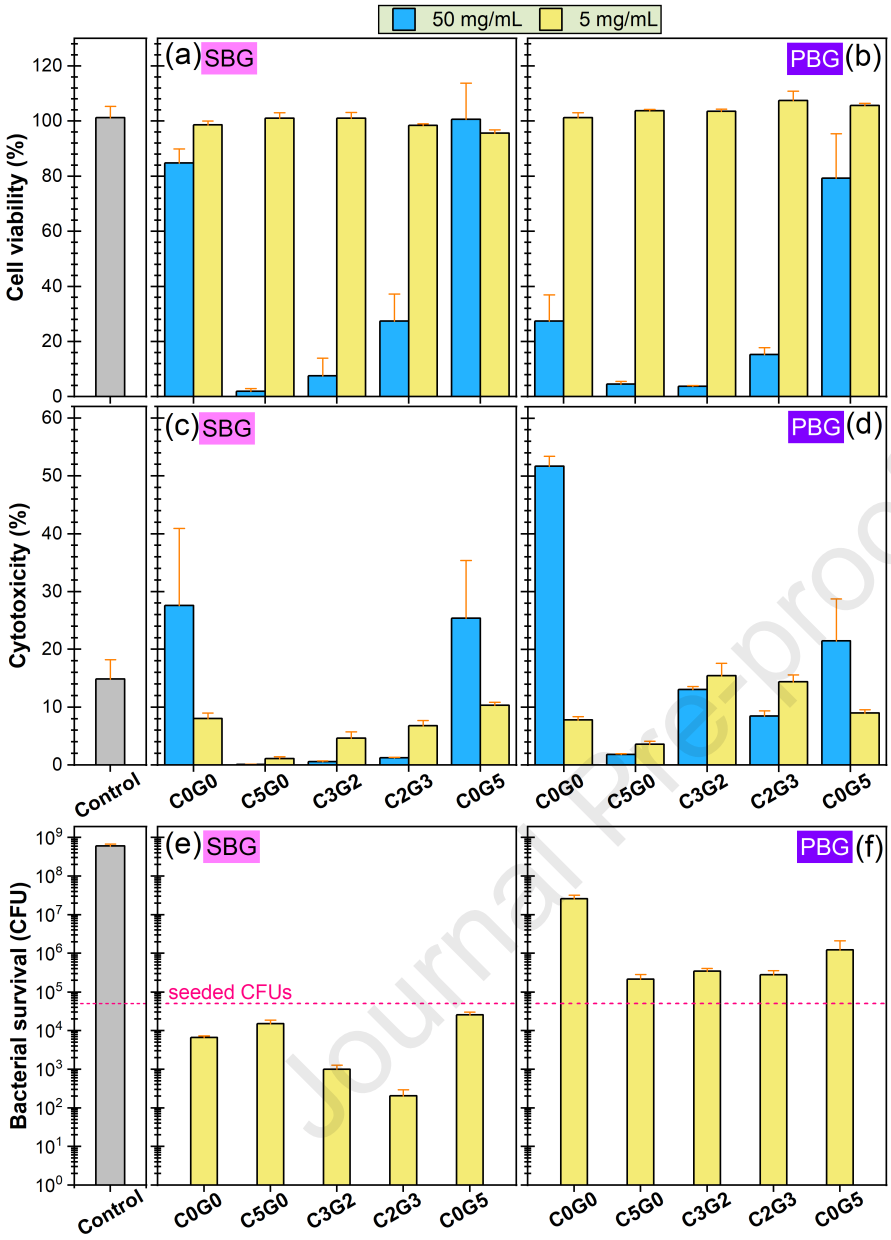

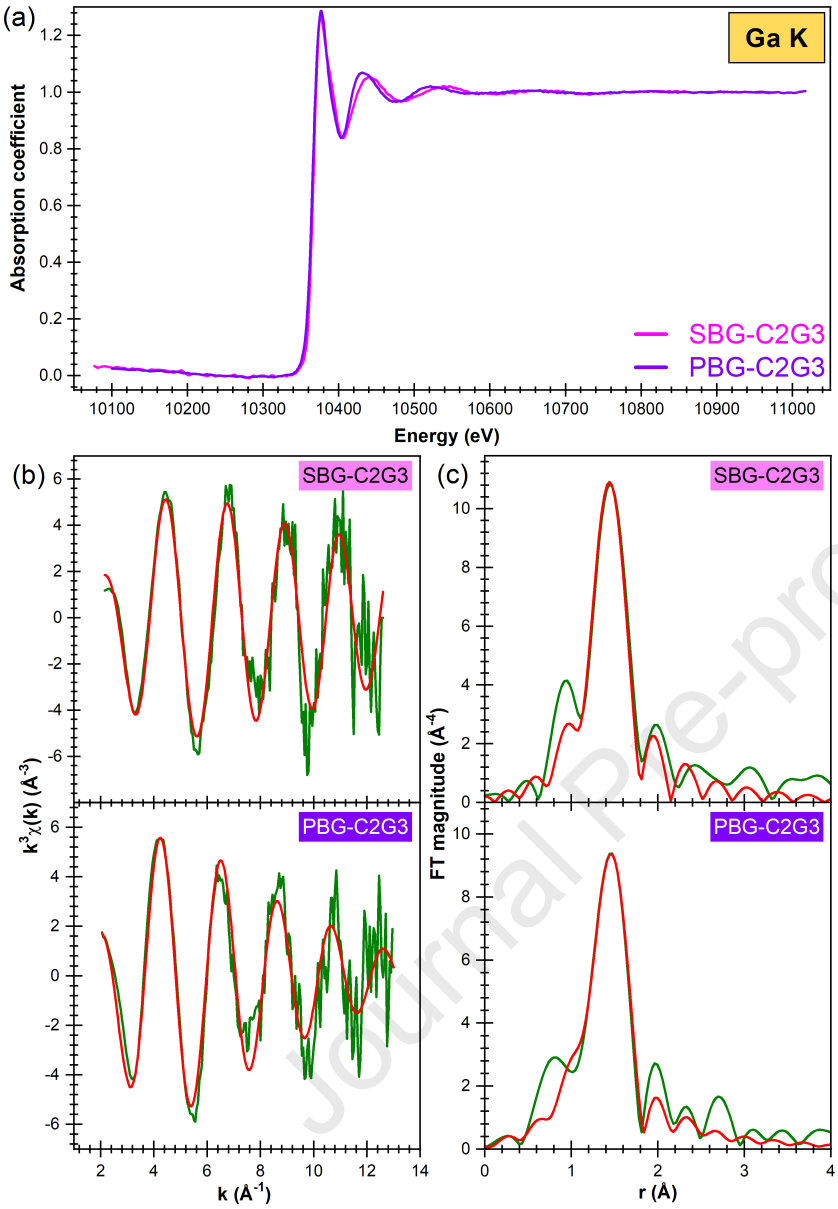

Highlights

- Cu and/or Ga doped silica (SBG) and phosphate (PBG) bio-glasses were synthesized.
- Ga played different structural roles dependent on glass host (SBG or PBG) matrix.
- Cu and Ga analogous or dissimilar structural roles governed their leaching rate.
- No cytotoxicity was shown at a powder-to-cell culture medium ratio of 5 mg/mL.
- The coupled Cu and Ga ion in SBG release stimulated the antimicrobial efficacy.

Conflict of Interest Form

We hereby declare that:

- All authors have participated to the (*i*) conception, design, and/or analysis and interpretation of the data; (*ii*) drafting the manuscript or revising it critically; and (*iii*) approval of the final version;

- This manuscript has not been submitted to, nor is under review at another journal;

- The authors have no affiliations with organizations with a direct or indirect financial interest in the subject matter discussed in the manuscript.

On behalf of all authors,
Dr. George Stan
National Institute of Materials Physics
Address: 405A Atomistilor street, 077125 Magurele-Ilfov, Romania
Office phone: +40-21-241-8128 / Mobile phone: +40-724-131-131
Fax: +40-21-369-0177
E-mail: george_stan@infim.ro

Magurele, 10th of November 2021

George E. Stan received the B.E. degree in medical engineering, the M.Sc. degree in biomaterials, and the Ph.D. degree in materials engineering from the University Politehnica of Bucharest, Bucharest, Romania, in 2005, 2007, and 2011, respectively. He is currently a Senior Researcher Rank I at the National Institute of Materials Physics, Magurele, Romania. His research interests are focused on the fabrication of quality thin films by physical vapour deposition techniques on large area or complex geometry substrates with applicative range in the field of biomedicine and electronics. His publication track record can be consulted at: https://publons.com/researcher/1367487. E-mail address: george_stan@infim.ro.

Declaration of interests

☒ The authors declare that they have no known competing financial interests or personal relationships that could have appeared to influence the work reported in this paper.

☐The authors declare the following financial interests/personal relationships which may be considered as potential competing interests:

On behalf of all authors,
Dr. George Stan
National Institute of Materials Physics
Address: 405A Atomistilor street, 077125 Magurele-Ilfov, Romania
Office phone: +40-21-241-8128 / Mobile phone: +40-724-131-131
Fax: +40-21-369-0177
E-mail: george_stan@infim.ro

Magurele, 10th of November 2021